Subsidence and exhumation of the Mesozoic Qiangtang Basin: Implications for the growth of the Tibetan plateau

Citation for published version:
Zhang, J, Sinclair, H, Li, Y, Wang, C, Persano, C, Qian, X, Han, Z, Yao, X & Duan, Y 2019, 'Subsidence and exhumation of the Mesozoic Qiangtang Basin: Implications for the growth of the Tibetan plateau', *Basin Research*, vol. 31, no. 4, pp. 754-781. https://doi.org/10.1111/bre.12343

Digital Object Identifier (DOI):
10.1111/bre.12343

Published In:
Basin Research

Subsidence and exhumation of the Mesozoic Qiangtang Basin: Implications for the growth of the Tibetan plateau

Journal:	*Basin Research*
Manuscript ID	BRE-020-2018.R3
Manuscript Type:	Original Article
Date Submitted by the Author:	n/a

Complete List of Authors:	Zhang, Jiawei; China University of Geosciences Beijing, State Key Laboratory of Biogeology and Environmental Geology; Institute of Geology, China Earthquake Administration, State Key Laboratory of Earthquake Dynamics Sinclair, Hugh; The University of Edinburgh, Grant Institute, School of GeoSciences Li, Yalin; China University of Geosciences Beijing, State Key Laboratory of Biogeology and Environmental Geology Wang, Chengshan; China University of Geosciences Beijing, State Key Laboratory of Biogeology and Environmental Geology Persano, Cristina; University of Glasgow College of Science and Engineering Qian, Xinyu; China University of Geosciences Beijing, State Key Laboratory of Biogeology and Environmental Geology Han, Zhongpeng; China University of Geosciences Beijing, State Key Laboratory of Biogeology and Environmental Geology Yao, Xiang; China University of Geosciences Beijing, State Key Laboratory of Geological Processes and Mineral Resources Duan, Yaoyao; Chengdu Centre of Geology and Mineral Resources

Keywords:	Qiangtang, Subsidence, Apatite fission track, Crustal thickening

Subsidence and exhumation of the Mesozoic Qiangtang Basin: Implications for the growth of the Tibetan plateau

Jiawei Zhang[a, b] Hugh D. Sinclair[c] Yalin Li[a,*] Chengshan Wang[a] Cristina Persano[d] Xinyu Qian[a] Zhongpeng Han[a] Xiang Yao[e] Yaoyao Duan[f]

[a] State Key Laboratory of Biogeology and Environmental Geology, China University of Geosciences (Beijing), Beijing 100083, China

[b] Now at State Key Laboratory of Earthquake Dynamics, Institute of Geology, China Earthquake Administration, Beijing 100029, China

[c] School of GeoSciences, University of Edinburgh, Drummond Street, Edinburgh EH8 9XP, Scotland, UK

[d] School of Geographical and Earth Sciences, College of Science and Engineering, University of Glasgow, Glasgow G12 8QQ, Scotland, UK

[e] State Key Laboratory of Geological Processes and Mineral Resources and College of Geosciences and Resources, China University of Geosciences (Beijing), Beijing 100083, China

[f] Chengdu Institute of Geology and Mineral Resources, Chengdu 610082, China

* Corresponding author.

Tel.: +086 10 82321586

Fax: +86 10 82321612

E–mail address: liyalin@cugb.edu.cn (Yalin Li)

ABSTRACT

The subsidence and exhumation histories of the Qiangtang Basin and their contributions to the early evolution of the Tibetan plateau are vigorously debated. This paper reconstructs the subsidence history of the Mesozoic Qiangtang Basin with eleven selected composite stratigraphic sections and constrains the first stage of cooling using apatite fission track data. Facies analysis, biostratigraphy, paleo-environment interpretation, and paleo-water depth estimation are integrated to create eleven composite sections through the basin. Backstripped subsidence calculations combined with previous work on sediment provenance and timing of deformation, show that the evolution of the Mesozoic Qiangtang Basin can be divided into two stages. From Late Triassic to Early Jurassic times, the North Qiangtang was a retro-foreland basin. In contrast, the South Qiangtang was a collisional pro-foreland basin. During Middle Jurassic to Early Cretaceous times, the North Qiangtang is interpreted as a hinterland basin between the Jinsha orogen and the Central Uplift; the South Qiangtang was controlled by subduction of Meso-Tethyan Ocean lithosphere and associated dynamic topography combined with loading from the Central Uplift. Detrital apatite fission track ages from Mesozoic sandstones concentrate in late Early to Late Cretaceous (120.9-84.1 Ma) and Paleogene-Eocene (65.4-40.1 Ma). Thermal history modelling results record Early Cretaceous rapid cooling; the termination of subsidence and onset of exhumation of the Mesozoic Qiangtang Basin suggest that the accumulation of crustal thickening in central Tibet probably initiated during Late Jurassic-Early Cretaceous times (150-130 Ma), involving underthrusting of both the

Lhasa and Songpan-Ganze terranes beneath the Qiangtang terrane, or the collision of Amdo terrane.

Keywords: Qiangtang, Subsidence, Apatite fission track, Crustal thickening

INTRODUCTION

The collision of India with Asia is the most important driving force for the growth of the Tibetan plateau (Argand, 1922; Dewey *et al.*, 1988; Yin & Harrison, 2000), with the onset of collision at about 55±10 Ma promoting significant changes in Tibetan plateau height and relief (Currie *et al.*, 2005; Rowley & Currie, 2006; Ding *et al.*, 2014, 2017; Wang *et al.*, 2014; Leary *et al.*, 2017). Evidence shows that deformation in the hinterland of the plateau occurred before collision (Murphy *et al.*, 1997; Kapp *et al.*, 2005). However, uncertainty remains as to whether this early shortening resulted in moderate or high elevations within the Tibetan plateau prior to the India-Asia collision (Zhang *et al.*, 2012 and references therein). It is reasonable to speculate that the crustal thickening in the central region of the Tibetan plateau had started before Cenozoic times (Zhao *et al.*, 2017). The Qiangtang Basin developed on the overriding plate between two major suture zones (the Bangong Lake-Nujiang suture zone, BNSZ, to the south and the Jinsha River suture zone, JRSZ, to the north, respectively), and is considered to record the early growth of the central Tibetan plateau (Song, 2012; Ren *et al.*, 2015; Zhao *et al.*, 2017). However, Early Mesozoic subsidence and pre-Cenozoic exhumation histories of the Mesozoic marine Qiangtang Basin are unclear, which hinders understanding of the early history of crustal thickening in central Tibet. This is due in large part, to the extremely remote locations and the strong Cenozoic structural deformation of the stratigraphic successions (Kapp *et al.*, 2003, 2005). Therefore, understanding of the Mesozoic history of the Qiangtang Basin is variable. The proposed mechanisms for basin subsidence are dominated by two competing models. It is proposed that either the basin formed in an extensional setting on the southern margin of Eurasia during Late Triassic to Early Cretaceous times (e.g., Wang *et al.*, 2004a; Song, 2012), or that it represents a foreland basin (e.g. Wang *et al.*, 2001; Li *et al.*, 2002). Published thermochronologic data from the Qiangtang Basin come mainly from the Qiangtang culmination (Rohrmann *et al.*, 2012; Zhao *et al.*, 2017), and sparsely from detrital sandstones (Wang *et al.*, 2008a; Wang & Wei, 2013; Ren *et al.*, 2015). Cooling ages of different thermochronometers range from Early Jurassic to Cenozoic, and the initial timing of plateau growth is thought to range from Early Cretaceous to Paleogene (Wang *et al.*, 2008a; Rohrmann *et al.*, 2012; Zhao *et al.*, 2017).

Present-day stratigraphic thicknesses are the products of cumulative changes in rock volume through time caused by subsidence and burial (Allen & Allen, 2005). Reconstructing the subsidence histories of sedimentary basins provides data to directly interrogate the tectonic evolution of a basin (e.g. Brunet *et al.*, 2003; Carrapa & Garcia-Gastellanos, 2005; Abadi *et al.*, 2008; Holt *et al.*, 2010, 2015; Kuhn *et al.*, 2010; Sciunnach & Garzanti, 2012; Abdullayev *et al.*, 2017; Dressel *et al.*, 2017; Silvia *et al.*, 2017; Tozer *et al.*, 2017). The most commonly applied method to recover the 1-D subsidence history of a sedimentary basin is “backstripping” (Watts & Ryan, 1976; Sclater & Christie, 1980), which relies on physical properties of the stratigraphic sequences (thickness and porosity), combined with depositional ages, paleobathymetry and eustsay at the time of accumulation. The exhumation of sedimentary basins is usually related to tectonic evolution, surface erosion and deep geological processes (Bernet *et al.*, 2001; Reiners & Brandon, 2006). Various thermochronometric systems have been used to provide important information on the timing and duration of cooling events that can be related to rock uplift and erosion of a sedimentary basin (Naeser *et al.*, 1989; Cederbom *et al.*, 2004; Armstrong, 2005).

This study carried out subsidence analysis of the Mesozoic Qiangtang Basin using stratigraphic successions obtained from geological surveys during the last three decades. New subsidence curves of the Qiangtang Basin established in this study suggest a transition from a foreland basin on the south of the JRSZ during Triassic times, to a hinterland basin (Horton, 2012) from Middle Jurassic to Early Cretaceous times. The cooling history of the basin is constrained using apatite fission track data from sandstones with modelling results indicating Early Cretaceous basin inversion and exhumation, which we interpret to be related to the collision of the Amdo basement or the initial amalgamation between the Lhasa and Qiangtang terranes. Our results contribute to the understanding of the evolution of the Qiangtang Basin and have implications for the Mesozoic growth of the Tibetan plateau.

GEOLOGIC BACKGROUND

The Tibetan plateau consists of several tectonic terranes, including the Himalayas, Lhasa, Qiangtang, Songpan-Ganze, and Kunlun-Qaidam, divided by several nearly east-west suture zones (Yin & Harrision 2000; Dai *et al.*, 2011; Zhang *et al.*, 2012). The Qiangtang terrane, located in the central part of the plateau, is delimited by the JRSZ to the north and the BNSZ to the south (Fig. 1a). The JRSZ is considered to represent the closure of the Palaeo-Tethys Ocean in Permian to Late Triassic times, which opened probably in Early Carboniferous or earlier (Dewey *et al.*, 1988; Pearce & Houjun, 1988; Kapp *et al.*, 2003; Zhai *et al.*, 2015). Middle to Upper Triassic deep-marine turbidites derived from surrounding blocks are preserved in the triangle-shaped Songpan-Ganze terrane north of the JRSZ (Nie *et al.*, 1994; Weislogel *et al.*, 2006; Ding *et al.*, 2013a). The Songpan-Ganze terrane was strongly deformed in the Late Triassic during closure of Paleo-Tethys (Chang, 2000; Roger *et al.*, 2011). Meanwhile, suturing along the JRSZ had taken place by Late Triassic (Norian) times, supplying a source of sediment southwards to the Qiangtang Basin (Li *et al.*, 2003). New geophysical and geochemical evidence reveal that the Songpan-Ganze complex may have subducted southward beneath the Qiangtang terrane along the JRSZ during Late Triassic (Zeng *et al.*, 2015; Lu *et al.*, 2017).

The BNSZ represents the closure of the Meso-Tethyan seaway along the southern margin of the Qiangtang terrane during Late Jurassic to Late Cretaceous times, resulting in amalgamation of the Lhasa and Qiangtang terranes (Fig. 1a) (Yin & Harrison, 2000; Kapp *et al.*, 2007; Zhu *et al.*, 2013, 2016; Fan *et al.*, 2015; 2016; Li *et al.*, 2016; Yan *et al.*, 2016; Chen *et al.*, 2017a; Huang *et al.*, 2017; Li *et al.*, 2017a; Liu *et al.*, 2017). Ophiolite fragments and Mesozoic clastic units (Li *et al.*, 2017b) within the BNSZ are tectonically superimposed. The Amdo basement (Fig. 1b) may have been isolated as a microcontinent or a continental arc during the formation of the

Bangong-Nujiang Meso-Tethyan Ocean ophiolites (Guynn *et al.*, 2006; Zhang *et al.*, 2014).

The Qiangtang Basin is subdivided into the North Qiangtang sub-basin, the Central Uplift, and the South Qiangtang sub-basin (Fig. 1b, Wang *et al.*, 2004b). The Central Uplift is composed of blueschist-bearing metamorphic mélange (Kapp *et al.*, 2000; Zhang *et al.*, 2006; Pullen & Kapp, 2014), Paleozoic low-grade strata (Kapp *et al.*, 2000), and Late Triassic intermediate to felsic intrusive rocks (Kapp *et al.*, 2000; Li *et al.*, 2015a). The contacts between metamorphic rocks and overlying Paleozoic-Triassic low-grade strata are low-angle normal faults (Kapp *et al.*, 2000, 2003). The formation of the Central Uplift is still an enigma, with interpretations ranging from an in-situ suture (Longmucuo-Shuanghu suture zone, LSSZ) (e.g., Li *et al.*, 1995; Zhang *et al.*, 2006; Liu *et al.*, 2011; Zhao *et al.*, 2014, 2015; Zhai *et al.*, 2015; Yan *et al.*, 2016; Liang *et al.*, 2017) to the underthrust model that the mélange was thrust beneath the Qiangtang terrane from the north and exhumed to the surface by large-scale core complexes (e.g., Yin & Harrison, 2000; Kapp *et al.*, 2000, 2003; Pullen & Kapp, 2014).

Despite the fact that the tectonic significance of the Central Uplift is debated, the Mesozoic stratigraphic sequences in both the North and South Qiangtang are well documented. In the North Qiangtang region they are separated by two major unconformities in Upper Triassic to Lower Jurassic and the Lower Cretaceous; while in the South Qiangtang region, the Mesozoic strata are complete until the Lower Cretaceous (Fig. 2). Lower and Middle Triassic strata are sparse throughout the entire

Qiangtang Basin. Upper Triassic sediments are represented by offshore to shallow marine limestones (Juhuashan Fm. of the North Qiangtang), deep marine flysch (Zangxiahe Fm.), and deltaic and littoral sandstones, siltstones and mudstones (Riganpeicuo Group of the South Qiangtang). The Nadigangri volcanic rocks overlie the paleo-weathering crusts in some places in the North Qiangtang (Fu et al, 2007; Wang *et al.*, 2007). This set of volcanic rocks was considered to record the onset of filling of the Mesozoic Qiangtang Basin (Wang *et al.*, 2004b; Fu *et al.*, 2010), and assigned to an Early Jurassic (Zhu *et al.*, 1996, 1997) or Middle Jurassic age (Wang *et al.*, 2001) until Zhai & Li (2007), Wang *et al.* (2008b) and Fu *et al.* (2010) presented SHRIMP zircon U-Pb ages of 219±4 Ma, 216±4.5 Ma and 220.4±2.3 Ma, respectively.

The Jurassic sequences are complete in both the northern and southern portions of the Qiangtang Basin, except that the Lower Jurassic units are missing in the North Qiangtang, while contemporaneous sequences in the South Qiangtang are represented by coastal black shales interbedded with limestones and gypsum (Quse Fm., Fig. 2). The earliest Middle Jurassic successions include tidal or deltaic coarse sediments (Qumocuo Fm. of the North Qiangtang) and shallow-marine black shales with limestones (Sewa Fm. of the South Qiangtang) (Wang *et al.*, 2004b). The upper sequences of the Middle Jurassic consist of marine platform limestones, dolomites (Buqu Fm., Ding *et al.*, 2013b) and regressional semi-closed tidal flat sediments (Xiali Fm., Song *et al.*, 2017). The Upper Jurassic unit is represented by intra-platform littoral-neritic carbonate rocks and black shales deposited in a closed, deep and static marine environment (Suowa Fm., Wang *et al.*, 2013).

During latest Jurassic to earliest Cretaceous times, the stratigraphic sequences are represented by clastic-carbonate sediments. The marine sedimentation in the North Qiangtang during the Early Cretaceous is represented by Xueshan Fm. and diachronous Bailongbinghe, Suowa and Xiali formations (Li & Batten, 2004; Yang *et al.*, 2017). Although Zhang (2000) and Zhang *et al.* (2004) asserted that the southern half of Qiangtang terrane was an area of marine sedimentation during Early Cretaceous, the marine sediments prevailed in its southern margin, close to the BNSZ. They have closer affinity to the BNSZ (Li *et al.*, 2017b) and are divided into different stratigraphic divisions (Mugagangri stratigraphic area) from the Jurassic sediments in the South Qiangtang. Overlying the repeated transgressive and regressive sequences (Ding *et al.*, 2013b) is a Lower Cretaceous unconformity. Upper Cretaceous alluvial and fluvial red sediments (Abushan Fm.) occupied the South Qiangtang depression, but are not found in its northern counterpart (Fig. 2). Its age has been defined to 102-75 Ma (Late Cretaceous) by different geochronological methods (Li *et al.*, 2013; Wu *et al.*, 2014; Li *et al.*, 2015c; Chen *et al.*, 2017b). Cenozoic terrestrial deposits unconformably overlie these Upper Cretaceous sequences.

METHODS

Backstripping and Data

The principle of backstripping analysis is an inverse modelling approach utilizing the stratigraphic record (Watts & Ryan, 1976; Sclater & Christie, 1980). Both the total and backstripped subsidence curves are time versus depth diagrams. In the actual operating process, the first step is stratigraphic correlations and age assessment, after which combining decompaction, palaeobathymetry and eustasy yield the total subsidence history. By removing the subsidence generated by sediment and water loads, the component of subsidence driven by tectonic forcing remains (Magoon & Dow, 1994; Stapel *et al.*, 1996). We used a MATLAB program (Yao *et al.*, 2017) to calculate the final tectonic subsidence and error bars.

Stratigraphic units

An issue is the poor exposure of the stratigraphic successions in the Qiangtang Basin where strong weathering and Cenozoic deformation (Kapp *et al.*, 2005) affect preservation. All the exploration wells, currently, are shallow ones (none deeper than 1.5 km) that encounter only a small part of the Mesozoic successions. Therefore, subsidence recovery was accomplished using surface sections. Geological survey institutes from China and our working group have measured up to 235 detailed stratigraphic sections in the Qiangtang Basin. The first step is integrating scattered sections into a composite successive column by lithologic or biostratigraphic correlations (Sciunnach & Garzanti, 2012). As many measured stratigraphic sections are hard to be integrated into one composite profile, because of the incomplete exposure of Mesozoic sequences in one depression or severe disturbance caused by Cenozoic deformation, we managed to restore eleven composite profiles in total (see the Supporting information for the GPS data of all 235 sections and precise locations of 11 composite profiles on Google Earth). For each of the eleven selected composite sections, the average thickness of the various sections was used among the numerous profiles in the same depression. The details of thickness of each stratigraphic unit are given in Table S1.

In the North Qiangtang, nine locations were chosen to conduct subsidence analyses, partly because the North Qiangtang occupies a large portion of the basin (Fig. 1). Most locations have disrupted sequences, except for Nadigangri and Quemo Co (Fig. 3). Three major unconformities can be found in strata exposed in the North Qiangtang (Figs. 2 and 4). All of the sections, at the bottom, are characterized by Upper Triassic marine limestones (Juhuashan Fm. of Duxue Mt., Shuangquan Lake, and Zuerkenwula Mt., and Bolila Fm. of Quemo Co), and clastic deposits (Zangxiahe Fm. of Heihuling and Changshui River, Tumengela Group of Dangmagang, and Bagong Fm. and Erlongba Fm. of Quemo Co), with the exception of the Nadigangri and Amugang sections which do not preserve marine deposits. The Amugang section is represented by Permian metavolcanic rocks which underlie the whole sequence. The first major gap appears between the marine deposits and overlying volcanic rocks (Nadigangri Fm.). This unconformity appears only in the western part of the North Qiangtang (Duxue Mt., Shuangquan Lake, Heihuling and Nadigangri), while the eastern portion only exhibits the second major unconformity, which is prevalent across the North Qiangtang. The second major unconformity is between Upper Triassic and Middle Jurassic strata. The Lower Jurassic units are missing in the North Qiangtang, suggesting a long-term hiatus or tectonic uplift after the closure of Jinsha River suture to the north. The Middle Jurassic successions include Qumocuo Fm., Buqu Fm. and Xiali Fm. (Fig. 4). The Upper Jurassic unit is represented by Suowa

Fm. During latest Jurassic to earliest Cretaceous, the stratigraphic sequences consist of clastic sediments, Bailongbinghe and Xueshan formations (Fig. 2). Note that the Bailongbinghe and Xueshan formations are probably contemporaneous heterotopic facies so that they are not both recorded in some locations. The last major unconformity is between Cenozoic fluvial and lacustrine Kangtuo Fm. and latest Jurassic to earliest Cretaceous sandstones. No Late Cretaceous sediments were discovered.

Two sites were considered ideal for modelling of subsidence histories of the South Qiangtang, the Biluo Co and Dazhuoma sections (Figs. 1 and 5). Mesozoic sequences are more complete than that of the North Qiangtang, with only one or two major unconformities recognized (Fig. 5). The Late Triassic sequences are represented by fine-grained clastic deposits (Riganpeico Group of Biluo Co and Adula Fm. of Dazhuoma), sandstones (Duogaila Fm. of Dazhuoma), and limestones (Suobucha Fm. of Biluo Co). It is noticeable that the Biluo Co section is complete, while the Dazhuoma section has an obvious unconformity between the Jurassic Quemocuo Fm. and the Triassic sandstones. This indicates an east-west difference in the paleogeography of the South Qiangtang. The early stage of the Jurassic sequences seems to record contemporaneous heterotopic facies in Biluo Co (Quse Fm. and Sewa Fm.) and Dazhuoma (Quemocuo Fm.), respectively. The discrepancy lies in the grain size and thickness where the Biluo Co section is finer and thicker (Fig. 5). The rest of the Jurassic sequences are characterized by limestones interbedded with sandstones, siltstones and mudstones. The lower limestone unit, Buqu Fm., preserves dolomites and gypsum, reflecting an arid period during a marine transgression-regression cycle. The upper limestone unit, Suowa Fm., is characterized by darker bioclastic limestone. The interbedded clastic unit is relatively fine grained. A regional unconformity appears above the upper limestone unit, with latest Jurassic to earliest Cretaceous clastic deposits missing in the South Qiangtang compared to that of the North Qiangtang (Figs. 4 and 5). The Late Cretaceous Abushan Fm. is only recognized in the South Qiangtang, which is unconformably overlay by Cenozoic Kangtuo Fm.

Age constraints

Hundreds of samples from regional geological surveys were studied for biostratigraphy (e.g., ammonoids, bivalves, corals, brachiopods, foraminifers, radiolarians, fusulinids, etc., see Table S2 in Supporting material for details about fossils and their constrained biostratigraphy), resulting in reliable biostratigraphic control (e.g., Chen *et al.*, 2016; Yin, 2016; Yin & Chandler, 2016) and refined palaeoenvironmental and palaeowater-depth interpretations. All Jurassic strata contain abundant bivalves to constrain ages (Table 1). In addition, ages of Jurassic sequences are constrained by magnetostratigraphy of Fang *et al.* (2016) (Fig. 2).

The accuracy of subsidence history plots heavily depends on the precision of age assessment. The choice of timescale is important when transforming relative ages derived from biotas into numerical ages. However, there are a few differences in recent timescales by different authors, and so we adopt the standard timescale of Gradstein *et al.* (2004) and Ogg *et al.* (2008).

Decompaction

The quantitative analysis of total subsidence history relies mainly on stepwise decompaction of stratigraphic units (Bond & Kominz, 1984). The principle of decompaction is based on the reduction of porosity with depth (Allen & Allen, 2005 and references therein). Generally the porosity decreases exponentially with depth (Steckler & Watts, 1978; Sclater & Christie, 1980):

$$\Phi = \Phi_o e^{-cy} \quad (1)$$

where Φ_o is the surface porosity, Φ is the porosity at the given depth y, and c is a lithology-dependent coefficient. The standard Φ_o and c values for different lithologies used in this study come from Sclater & Christie (1980).

In the decompaction process, when recovering the depths y_1 and y_2 of the sedimentary unit to its initial uncompacted depths y_1' and y_2' (Fig. 6), the decompacted thickness H, will be the following result (Allen & Allen, 2005):

$$H = y_2' - y_1' = y_2 - y_1 + \Phi_o[(e^{-cy1'} - e^{-cy2'}) - (e^{-cy1} - e^{-cy2})]/c \quad (2)$$

where $\Phi_o(e^{-cy1'} - e^{-cy2'})/c$ is the pore volume after decompaction, and $\Phi_o(e^{-cy1} - e^{-cy'})/c$ is the pore volume before decompaction.

Backstripping

The total subsidence is divided into two parts, one resulting from the tectonic driving forces and the other caused by sediment and water loads. The subsidence curve obtained after decompaction is the total subsidence (Watts *et al.*, 1982; Busby & Ingersoll, 1995). Sediment load must be subtracted by means of isostatic models (Einsele, 1992). An Airy isostastatic model was adopted in this study.

In an Airy isostastatic model, the tectonic subsidence, D, can be backstripped from H using the equation given by Watts & Ryan (1976):

$$D=H(\rho_m-\rho_s)/(\rho_m-\rho_w) \quad (3)$$

where ρ_m, ρ_s, and ρ_w are densities of lithospheric mantle, sediments and water, respectively. Values for ρ_m and ρ_w are constant and we adopt 3.33 and 1.035 g/cm^3 for each of them. Values for ρ_s are calculated in terms of weighted mean average densities of different lithologies during progressive decompaction using the following equation (Allen & Allen, 2005):

$$\rho_s=\Sigma\{[\Phi_i\cdot\rho_w+(1-\Phi_i)\,\rho_{sgi}]/H\}Y_i' \quad (4)$$

where Φ_i is the porosity of a specific layer, ρ_{sgi} is the sediment grain density of one layer, and Y_i' is the thickness of layer i.

Boundary conditions

Sea-level changes and paleo-water depths are usually used as boundary conditions in modelling. Although regional sea-level changes often differ from global scales, global sea-level curves are used in many cases. We adopt the eustatic sea-level curves of Miller *et al.* (2005) for Mesozoic eustatic corrections. The eustasy data are given in Table S1.

Paleo-water depth often has a wide range of uncertainty (e.g., Bertram & Milton, 1988) and are derived primarily from fossils, sedimentary structures, geochemical signatures (values and ratios of trace, transition and rare earth element, etc.), and depositional environment interpretations (Sciunnach & Garzanti, 2012) (Fig. 7). For instance, the biomarkers of the Middle Jurassic Buqu Formation indicate an offshore to shallow marine environment (Chen *et al.*, 2014), which suggested a paleo-water depth of 0-150 m. All the paleo-water depths used in the modelling are listed in Table S1 in Supplementary material.

After corrections for paleo-water depth and variations in sea-level change are conducted, the Airy compensated tectonic component of basement subsidence, Y, is (Sclater & Christie, 1980):

$$Y=D+W_d-\Delta_{sl}\cdot\rho_m/(\rho_m-\rho_w) \qquad (5)$$

where W_d is the assumed paleo-water depth, and Δ_{sl} is paleo-sea level relative to the present.

The uncertainties of backstripping methods

Generally, the uncertainty of stratigraphic thickness is small. It mostly comes from the unknown amount of erosion at unconformities. The apatite fission track analyses could constrain the erosion thickness in the Dazhuoma section (Figs. 1 and 5;

Table 2). However, it can not be applied to the other sections. As a result, this correction was neglected, as assessment of the amounts of erosional removal are not accessible in these sections; it is recognized that this provides uncertainty in the final subsidence calculation.

Age assessment has a large uncertainty because most of the age constraints derive from biostratigraphy. Only the volcanic rocks of Late Triassic Nadigangri Fm. are constrained by U-Pb zircon dating. The uncertainty in age assessment causes little change to the shape of subsidence curves. The biostratigraphy information of all the sequences are tabulated in Table S2 in Supplementary material.

Paleo-water depth often has a wide range of uncertainty, especially for deep-water units (Sciunnach & Garzanti, 2012). In our study, paleo-water depths are based on the interpretation of paleo-environment and have large errors on them. Sea-level corrections are based on curves generated from the Atlantic passive margin (Miller *et al.*, 2005), which may differ from regional sea-level histories linked to variations in the geoid.

Finally, the use of a simple Airy isostatic correction is applied as there is uncertainty around the flexural rigidity of the plate during the Mesozoic loading. The implication is that the rates of tectonically induced subsidence following backstripping would have been greater, but the pattern of subsidence unchanged (Allen and Allen, 2005).

Apatite Fission Track Thermochronology

Materials and methods

12 sandstone samples were collected for apatite fission track (AFT) analyses (Fig. 1; GPS coordinates are given in Table S3 in Supplementary material). Seven samples came from the Amugang, Biluo Co and Dazhuoma sections (Figs. 4 and 5). The other five were from geological surveys. Fission track ages, track lengths, and *D*par (etched pits of fission tracks on a polished surface) measurements were performed at the University of Glasgow using the external detector method (Gleadow, 1981; Donelick *et al.*, 2005) and the zeta calibration technique (Huford & Green, 1983), following the techniques provided by Persano *et al.* (2005). Apatite grains were etched for 20 s in 5.0 M HNO_3 at room temperature (~20°C). Mica detectors were etched with HF for 25 min. Samples were irradiated at Oregon State TRIGA Reactor, USA. Apatites were irradiated together with IRMM 540R dosimeter glasses to check the constancy of the neutron flux. The samples and standards were counted under a Carl Zeiss Axio Imager M1m optical microscope at 1250 × magnification and the FTStage 4.04 system by Trevor Dumitru. All AFT data were processed and plotted using TrackKey software (Dunkl, 2002); their populations were analyzed using Density Plotter (Vermeesch, 2012). The χ^2 test (Galbraith, 1981; Green, 1981) was performed on all samples to determine the populations in a grain-age distribution.

Thermal History Modelling

HeFTy, a Monto Carlo approach to data interpretation (Ketcham *et al.*, 2005), was used to decipher thermal history. Fission track age and track length were modelled using the multi-kinetic annealing model of Ketcham *et al.* (2007), using *D*par as a kinetic parameter (Donelick *et al.*, 2005). Inverse thermal history modelling was run until 100 good paths were obtained, which in all cases resulted >10000 acceptable paths.

RESULTS

Subsidence History

Subsidence history of the nine locations in the North Qiangtang and two in the South Qiangtang were generated (Fig. 8). A total decompacted subsidence curve and a backstripped, tectonic subsidence curve were obtained for each site.

All curves of the North Qiangtang show two stages of concave-up subsidence, a lower magnitude during Late Triassic and a more pronounced stage during Middle Jurassic to Early Cretaceous. In the first stage, rapid tectonic subsidence was recorded during middle Late Triassic, followed by a deceleration or termination in tectonic subsidence. To more clearly understand the latter stage of subsidence history, we focus on the subsidence curves from ~172 Ma to 120 Ma (Fig. 9). This stage of subsidence started at around 172 Ma, with subsidence curves that are either concave or nearly liner (e.g., Duxue Mt. and Shuangquan Lake). The last phase of most subsidence curves decelerate with time with the exception of Duxue Mt. and Shuangquan Lake (Fig. 9). A suspension was recorded in the Heihuling profile at about 165 Ma.

Two sites in the South Qiangtang show distinct subsidence patterns. The subsidence rate of Biluo Co accelerated with time at first, and then decelerated in the Late Jurassic (Fig. 8). In contrast, the subsidence curve of Dazhuoma shows a two-stage evolution, which is similar to those in the North Qiangtang.

Apatite Fission Track

Central ages of all sandstone samples range from 120.9 ± 5.5 to 40.1 ± 2.6 Ma (Table 2), which are much younger than the stratigraphic ages (Triassic-Cretaceous). The grain-age distributions can be divided into two groups. One is late Early to Late Cretaceous (120.9-84.1 Ma) and another is Paleogene-Eocene (65.4-40.1 Ma). Four samples (ED0616, EP1502, EP1504-17 and PQ1503) failed the χ^2 test, suggesting that the apatite composition may vary significantly within each sample (O'Sullivan & Parrish, 1995) and they may have multiple age populations. The age dispersion of these four samples are moderate to high (> 20%) (Table 2). Despite failing the χ^2 test, a mixture model (Galbraith & Green, 1990) does not show two populations for the majority of samples, with exception of sample EP1502 (Fig. 10). The relatively short mean horizontal confined track lengths (MTLs) range from 9.26 ± 0.39 to 13.75 ± 0.48 μm (Table 2). This pattern suggests that these samples were buried within the partial annealing zone of AFT, or reheated for a long time before exhumed to the surface. Most samples have limited amount of horizontal confined tracks. Therefore, it is difficult to extract useful information from MTLs. *D*par values range from 1.74 to 3.49 μm, with many incomparable with Durango apatite (2.05±0.16 μm, Sobel & Seward, 2010), which means many samples have different compositionally controlled annealing properties compared with Durango apatite. The relatively large *D*par values reflect the high values of Cl wt% (>1-2 wt%, Donelick *et al.*, 2005 and references therein) in these samples, which suggests relatively slow annealing of apatite grains (Donelick *et al.*, 2005; Galbraith, 2005).

Thermal History Modelling

Three initial constraints were applied to four sandstone samples that were selected to run modelling: (1) temperature of 5 ± 5 °C for the present surface; (2) temperature of 20 ± 20 °C for the depositional ages, which were constrained by magnetostratigraphy of Fang *et al.* (2016); (3) temperature of 120-200 °C between 160-120 Ma, which is constrained by subsidence history, adopting a geothermal gradient of 30 °C/km (He *et al.*, 2014). Modelling results of four samples (ED0616, EP1502, PQ1503 and PQ1506) from the Qiangtang Basin indicate a relatively simple cooling history (Fig. 11; see Figure S1 for all thermal history models). After deposition, all samples reached maximum temperature 150-170 °C at about 150-130 Ma, which is much higher than the base of the apatite partial annealing zone (110 ± 10 °C, Ketcham *et al.*, 1999), suggesting entire reset apatite fission track ages. Cooling started at about 140-130 Ma, which is coincident with the timing of crustal thickening inferred from the subsidence history. After *ca.* 100 Ma, all the samples present protracted cooling histories, followed by increase in cooling rates, up to 2-5 °C Myr^{-1}, at *ca.* 25-10 Ma.

DISCUSSION

Subsidence Analyses of the Mesozoic Qiangtang Basin

Based on the subsidence histories (Figs. 8 and 9) combined with previous work on sediment provenance (Fig. 12) and timing of deformation, we suggest that the evolution of the Mesozoic Qiangtang Basin can be subdivided into two main stages, Late Triassic-Early Jurassic and Middle Jurassic-Early Cretaceous.

Late Triassic-Early Jurassic

The North and South Qiangtang may have been separated by the paleo-Tethys Ocean before the Triassic (Li *et al.*, 1995; Song *et al.*, 2017). The North Qiangtang was a foreland basin in the early Late Triassic to the south of the JRSZ (Li *et al.*, 2003; Song, 2012), which resulted from the collision between the Songpan-Ganze and Qiangtang (Yan *et al.*, 2016) (Fig. 13a). Li *et al.* (2003) proposed that the main paleo-current directions at the northern edge of the North Qiangtang region were southwestward, and the turbidites and delta sandstones transitioned to thinner and finer foredeep sediments from north to south when marine Juhuashan and Zangxiahe formations were deposited. Additionally, the Carnian mudstones were deposited under a collisional setting based on the multi-major elements discriminate plots (Wang *et al.*, 2017a). The subsidence history patterns of the North Qiangtang are concave-upward during early Late Triassic (grey-shaded area in Fig. 8), which is consistent with the characteristics of subsidence curves of retro-foreland basins (Naylor & Sinclair, 2008), though the subsidence is not remarkable and the error bars may make the data less reliable. We interpret that the marine deposits in the North Qiangtang were generated from flexural subsidence by orogenic loading in the JRSZ in the early Late Triassic (Fig. 13a).

Provenance analyses and paleo-current directions indicate that the JRSZ had been a topographic highland and source area by the end of Late Triassic when the Nadigangri volcanic rocks formed (Li *et al.*, 2003). The presence of paleo-weathering crusts (Fu et al, 2007; Wang *et al.*, 2007), marking the termination of early Late

Triassic subsidence, means that the North Qiangtang was subaerially exposed in the Late Triassic. The Nadigangri volcanic rocks (~216-220 Ma) unconformably overlay the paleo-weathering crusts after the early Late Triassic subsidence ceased. The majority of these volcanic rocks are felsic, rather than basaltic. As a result, we interpret these, like other bimodal magmatism found in the North Qiangtang (Zhang *et al.*, 2011), to be a result of the detachment and sinking of oceanic lithosphere of the South Qiangtang in the Late Triassic (Zhai & Li, 2007; Zhai *et al.*, 2013) (Fig. 13b), but not as the onset of a rift basin (e.g., Fu *et al.*, 2010). The tectonic subsidence that accommodated the Nadigangri volcanic rocks (Fig. 8) is interpreted as subsidence due to local lithospheric stretching based on geochemical analyses of Fu *et al.* (2010). The North Qiangtang had been an area of erosion since the paleo-weathering crusts formed and it exhibits unconformities lasting about 50 m.y. on the tectonic subsidence curves (Fig. 8).

Although the large error bars also makes the data less reliable, the accelerating subsidence curve of Biluo Co in the South Qiangtang shows a unique characteristic of collisional pro-foreland basins (Kneller, 1991; Miall, 1995; DeCelles & Giles, 1996; Naylor & Sinclair, 2008) (Fig. 8). One possible explanation is that it evolved on the south of the Central Uplift mountain belt as the South Qiangtang collided with the North Qiangtang. (Li *et al.*, 1995; Liu *et al.*, 2011; Zhao *et al.*, 2014, 2015; Yan *et al.*, 2016; Liang *et al.*, 2017) (Fig. 13a). The convex-upward tract of the subsidence curve for Biluo Co demonstrates that local forces, the northward subduction of the South Qiangtang lithosphere and the growth of Central Uplift, probably played an important role in controlling the development of the basin, just as other collisional foreland basins worldwide (e.g., North Alpine Foreland Basin of Homewood *et al.* (1986) and Ebro basin of Vergés *et al.* (1998)). New geochronology shows that the metamorphism in Central Uplift occurred at about 243-233 Ma (Pullen *et al.*, 2008; Dan *et al.*, 2018), marking the collision between the South and North Qiangtang. Subsequent exhumation occurred at 220-202 Ma (Kapp *et al.*, 2003; Dan *et al.*, 2018), which was synchronous with the commencement of subsidence at Biluo Co. Therefore, Late Triassic subsidence in the western part of South Qiangtang is interpreted to be caused by orogenic loading from the Central Uplift and static loads from the slab pull (Figs. 13a, b). However, in the east, the Dazhuoma site in the South Qiangtang shows a concave pattern of subsidence, which is similar to that of the North Qiangtang (Fig. 8). This suggests that there is a significant difference in basin evolution between east and west portions of the South Qiangtang during this time interval. In the eastern part (Dazhuoma), the Central Uplift was not created (Figs. 13a, b) and we interpret the subsidence arose from dynamic subsidence. As the shallowly subducting Paleo-Tethyan oceanic slab approached the South Qiangtang in the eastern part (Lu et al., 2017), it potentially caused viscous mantle flow that drove the subsidence (Fig. 13a). We ascribe differences between the eastern and western portions of South Qiangtang to the irregular shape of continental margin (Zhang & Tang, 2009) and varying subducting angles of Paleo-Tethyan oceanic slab (Lu *et al.*, 2017) (Fig. 13a).

Middle Jurassic-Early Cretaceous

The Middle Jurassic to Early Cretaceous is the main period of subsidence in the Mesozoic Qiangtang Basin. The Qiangtang terrane had been entirely accreted onto the southern margin of Eurasia since Early Jurassic (Dewey *et al.*, 1988; Pearce & Houjun, 1988). The Central Uplift has been an area of active exhumation based on provenance analysis and tectonic analyses (Li *et al.*, 2001; Kapp *et al.*, 2003) (Fig. 12). In addition, the denudation of the ultrahigh-pressure (UHP) metamorphic rocks in the Central Uplift is associated with lithospheric detachment and associated orogenic collapse (Zhang & Tang, 2009) (Fig. 13c). The thrust belt loading from both the south and north sides of the North Qiangtang potentially resulted in renewed subsidence. In addition, the northward subduction of Bangong-Nujiang oceanic lithosphere during 180-150 Ma (Liu *et al.*, 2017) may have resulted in viscous corner flow beneath the North Qiangtang (Fig. 13c). The subsidence started at around 172 Ma, and the rapid subsidence of Duxue Mt. and Shuangquan Lake (Fig. 9) may have resulted from additional sediments supply from the Central Uplift (Figs. 1 and 12).

The subsidence patterns resemble exponentially decaying thermal subsidence curves formed in extensional settings (Steckler & Watts, 1978; Christie-Blick & Biddle, 1985) and retro-foreland basins (Naylor & Sinclair, 2008; Sinclair & Naylor, 2012), or are associated with hinterland basins that show fast subsidence in very short time interval (Horton, 2018). Such a high rate of subsidence generated through extension would require β values to be over 2 (assuming homogeneous lithospheric extension of a 33 km thick crust), which would have generated oceanic lithosphere (Kneller, 1991), but no evidence is recorded. Moreover, no evidence of extensional

551 structures was found during Middle Jurassic to Early Cretaceous, such as
552 syndepositional normal faults. Currently, all the discovered normal faults in central
553 Tibet formed in Cenozoic times (e.g., Blisniuk *et al.*, 2001; Wang *et al.*, 2010; Ou *et*
554 *al.*, 2017). In addition, no volcanic rocks, particularly basaltic rocks, are found in the
555 Middle to Late Jurassic deposits. Therefore, we exclude lithospheric extension as the
556 mechanism. Based on the subsidence histories combined with previous work on
557 sediment provenance and timing of deformation, we prefer to interpret this stage of
558 the North Qiangtang as a hinterland basin controlled by renewed crustal thickening,
559 and loading from both the south and northern margins during Middle Jurassic-Early
560 Cretaceous. This interpretation is supported by several lines of evidence. First, Li *et al.*
561 (2001) reconstructed the paleogeomorphology and palaeogeography, based on
562 paleo-current directions, composition of lithic fragments in sandstones and
563 provenance analysis (Fig. 12). The molasses preserved in the Quemocuo Fm. (Fig. 4)
564 represented the initiation of subsidence in the North Qiangtang. The composition of
565 the overlying sandstones is consistent with deposition in a collisional setting in the
566 light of multidimensional tectonic discrimination based on major element analysis
567 (Wang *et al.*, 2017b). Sandstone modal analyses indicate the influx of sediments from
568 a recycled orogen source (Li *et al.*, 2001). Combined with paleo-current directions,
569 mainly southward and southwestward, the main source of the sediments must be the
570 JRSZ to the north, and some detritus derived from the exhumation of tectonic
571 culmination (the Central Uplift) in the basin (Fig. 12). In addition, the coarse
572 sediments are distributed mainly along the edges of the North Qiangtang, suggesting

the tectonic loads on both sides were the main driving force for subsidence (Li *et al.*, 2001). Second, the thickness of marine sediments is 6-8 km in the north and 4-5 km in the south (Fig. 8). It means that there were other driving forces on the south to accommodate such thick sediments. This could occur in hinterland basins where there is thrust loading from both sides of the basin (Horton, 2012). Additional subsidence in the north may have been generated by dynamic loading, because it is where the corner flow drag is concentrated (Mitrovica *et al.*, 1989) (Fig. 13c). In addition, the flat subduction of Meso-Tethyan Ocean slab potentially transmitted strain in to the hinterland driving renewed crustal thickening, loading and marine transgression. Third, the average accumulation rate of sediments during this time was about 0.2 km/Ma, with some locations (Shuangquan Lake and Duxue Mt.) over 0.45 km/Ma. This accumulation rate is consistent with that obtained for the Buqu Formation at Well QZ11 (0.15-0.395 km/Ma with optimal value of 0.268 km/Ma, Cheng *et al.*, 2017). The high accumulation rates in a short time interval resemble those for Andean hinterland basins (Horton, 2018 and references therein). In summary, the subsidence of the North Qiangtang was controlled by the combined mechanisms of flexural subsidence from both the Jinsha River orogen and the Central Uplift and long-wavelength dynamic subsidence caused by northward shallow subduction of Meso-Tethyan Ocean lithosphere (Fig. 13c).

In the South Qiangtang, the subsidence curves show similar characteristics with the North Qiangtang during Middle Jurassic to Early Cretaceous times. The subsidence rates are also equal to those in the south of the North Qiangtang. We interpret the subsidence in the South Qiangtang came from the subduction of Meso-Tethyan Ocean lithosphere and tectonic loading from the Central Uplift (Fig. 13c).

The deceleration in the last phase of subsidence might have resulted from the closure of the Bangong-Nujing Ocean or the onset of Lhasa-Qiangtang collision during Late Jurassic to Early Cretaceous (Yan *et al.*, 2016; Zhu *et al.*, 2016; Li *et al.*, 2017b). At about 148 Ma, subsidence terminated across the Qiangtang Basin. The beginning of exhumation of the Qiangtang Basin (Fig. 11) and the termination of subsidence happened simultaneously, probably indicating the onset of crustal thickening in the Qiangtang terrane.

Cretaceous

All subsidence curves in the North Qiangtang show the same trend with the Late Jurassic patterns that no subsidence is displayed (Fig. 8). No Late Cretaceous sediments are recorded. It was highly possible that the North Qiangtang started to show first stage of crustal thickening according to the thermal modelling results (PQ1503; Fig. 11).

The South Qiangtang records Late Cretaceous subsidence (Fig. 8). We interpret the Late Cretaceous Abushan Fm. as a response to the collision between Lhasa and Qiangtang terranes to the south (Yin & Harrison, 2000; Kapp *et al.*, 2007; Zhu *et al.*, 2013, 2016) (Fig. 13e), or to the collision of the Amdo terrane (Guynn *et al.*, 2006) (Fig. 13d). The oldest apatite fission track age (120.9 ± 5.5 Ma) may record the collision between the two terranes.

Implications for Pre-Cenozoic Evolution of the Tibetan Plateau

The timing of the topographic evolution of the Tibetan Plateau is still uncertain, though the general consensus is that central Tibet and surrounding areas had attained high elevation by 45 Ma or earlier (Murphy *et al.*, 1997; Kapp *et al.*, 2005, 2007; Rowley & Currie, 2006; Wang *et al.*, 2008a, 2014; Rohrmann *et al.*, 2012; Chen *et al.*, 2013; Xu *et al.*, 2013; Ding *et al.*, 2014; Tang *et al.*, 2017). Is the India-Asia collision strong enough to produce such high elevation and thickened crust in a very short period of time? The hinterland of the Tibetan plateau shows both a cessation of subsidence and an acceleration of exhumation recorded in zircon (U-Th)/He ages in the South Qiangtang (Zhao *et al.*, 2017) and apatite fission track modelling (Fig. 11), consistent with topographic growth at *ca.* 148 Ma. Mesozoic sediments were exhumed from >6 km depth at about 140-130 Ma, with exhumation rate of 0.1-0.3 mm/a (Fig. 11). This cooling event is also in agreement with accelerated cooling reflected by Late Jurassic-Cretaceous apatite fission ages from sedimentary rocks across the Qiangtang terrane (Wang & Wei, 2013; Ren *et al.*, 2015). This incident may mark the first stage of exhumation driven by crustal thickening in central Tibet (Zhao *et al.*, 2017). We ascribe the exhumation in central Tibet to the onset of continental collision between Lhasa and Qiangtang terranes, probably involving underthrusting of the Lhasa terrane beneath the Qiangtang terrane. Concurrent crustal thickening with collision suggests that the impact of the collision between Lhasa and Qiangtang terranes was potentially more profound than previously thought. The Jinsha River suture zone also played a role that can not be ignored, because both the Songpan-Ganze and Lhasa terranes may have been involved in underthrusting beneath the Qiangtang terrane. Alternatively, the Late Jurassic-Early Cretaceous exhumation (Fig. 11) or crustal thickening could be related to collision of the Amdo terrane caused by northward continental underthrusting of the Lhasa terrane (Guynn *et al.*, 2006) (Fig. 13d). The Amdo basement was interpreted to be exposed only at the central part of BNSZ, but buried in all other places (Guynn *et al.*, 2006). Recently, Li *et al.* (2017c) reported the existence of a destroyed Amdo-Tongka block through study along the eastern segment of BNSZ. Therefore, there may be an unrecognized block south of the Qiangtang terrane. Both scenarios suggest that the underthrusting of the Lhasa terrane contributed to the rapid exhumation or crustal thickening in central Tibet at about 150-130 Ma.

As shown in Figs. 8 and 9, the tectonic subsidence curves show no subsidence since the beginning of the Cretaceous, with cessation of marine deposition. At this time, the North Qiangtang started to record substantial crustal thickening and increased elevations. Cretaceous apatite fission track ages (120.9-84.1 Ma) reflect exhumation caused by a strong compressive episode (Rohrmann *et al.*, 2012; Ren *et al.*, 2015). Large magnitudes of convergence after ~100 Ma were documented between Lhasa and Qiangtang using paleomagnetic data (Chen *et al.*, 2017b), which is coeval with protracted cooling histories (Fig. 11). This event slightly lagged behind the closure of the BNSZ south of Qiangtang, which indicates that the crustal thickening of central Tibet was a result of continued convergence between Lhasa and Qiangtang. The cooling ages of Paleogene-Eocene (65.4-40.1 Ma) may reflect the early impact of the India-Asia collision on the Qiangtang, which probably involved underthrusting of greater Indian lithosphere as far north as the Qiangtang terrane (Rohrmann *et al.*, 2012).

CONCLUSIONS

We have conducted backstripping of basin stratigraphy and thermochronological analyses of Mesozoic sandstones to study the subsidence and exhumation of the Qiangtang Basin. The results not only reveal the evolution of the Mesozoic Qiangtang Basin, but also yield insight into the early growth of the Tibetan Plateau.

Based on the subsidence histories, combined with previous work on sediment provenance, timing of deformation, and thermochronologic data, we suggest that the evolution of the North Qiangtang sub-basin can be subdivided into two main stages. The first stage is Late Triassic to Early Jurassic and the second is Middle Jurassic to Early Cretaceous. In the early Late Triassic, the marine deposits were generated from flexural subsidence by orogenic loading in the JRSZ. Whereas the Nadigangri volcanic rocks were accommodated by thermal subsidence caused by local lithosphere stretching during Late Triassic. During the second stage, the subsidence was controlled by flexural subsidence from active shortening in the Central Uplift and the southern edge of the Jinsha orogeny, combined with long-wavelength dynamic subsidence caused by shallowly northward subduction of Meso-Tethyan Ocean lithosphere. Both stages are characterized by concave-upward subsidence curves. Initiation of exhumation reflected by thermal history modelling in the Early Cretaceous, may represent crustal thickening in central Tibet.

The subsidence of the South Qiangtang sub-basin can also be subdivided into two stages. The first stage (Late Triassic-Early Jurassic) in the western part is represented by an accelerating pattern of subsidence, which is typical of a collisional pro-foreland basin. This was caused by orogenic loading from the Central Uplift and static loads from the slab pull. Whereas in the eastern part, the subsidence was interpreted to come from dynamic loading caused by viscous mantle flow. The second stage (Middle Jurassic-Early Cretaceous) was controlled by the subduction of Meso-Tethyan Ocean lithosphere and tectonic loading from the Central Uplift.

The cessation of tectonic subsidence curves and initiation of cooling indicated in the thermal modelling histories may represent the first stage of rapid exhumation or crustal thickening in central Tibet at about 150-130 Ma. The central part of the plateau had probably begun to accumulate substantial crustal thickening and elevation, probably driven by underthrusting of both the Lhasa and Songpan-Ganze terranes beneath the Qiangtang terrane, or the collision of the Amdo terrane. The growth of the Tibetan Plateau may have begun before the India-Asia collision.

ACKNOWLEDGEMENTS

We acknowledge Dr. Nadine McQuarrie, Dr. Alexander Robinson, Dr. Paul Kapp, and two other anonymous reviewers for their constructive reviews and feedbacks. We would like to thank Dr. Pengfei Ma for the instructions in modelling. We also thank our Tibetan compatriots, Danzhen and Bazhu, who did a lot of favor in field work. We thank Dr. Zhiming Duan who provided information about boreholes in

Qiangtang. This research was financially supported by Ministry of Science and Technology of the People's Republic of China (2017YFC0601400-05), the China Geological Survey Project (DD20160027) and National Natural Science Foundation of China (41572188).

REFERENCES

ABADI, A.M., WEES, J.-D.V., DIJK, P.M.V. & CLOETINGH, S.A.P.L. (2005) Tectonics and Subsidence Evolution of the Sirt Basin, Libya. AAPG Bulletin, 92, 993-1027.

ABDULLAYEV, N.A., KADIROV, F. & GULIYEV, I.S. (2017) Subsidence History and Basin-Fill Evolution in the South Caspian Basin from Geophysical Mapping, Flexural Backstripping, Forward Lithospheric Modelling and Gravity Modelling. Geological Society, London, Special Publications, 427, 175-196.

ALLEN, P.A., ALLEN, J.R. (2005) Basin Analysis, Principles and Applications, second edn. Blackwell Publishing, Oxford, UK.

ARGAND, E. (1922). La Tectonique De L'asie. Congrès géologique international (XIIIe session), Belgique.

ARMSTRONG, P.A. (2005) Thermochronometers in Sedimentary Basins. Low-Temperature Thermochronology: Techniques, Interpretations, and Applications, 58, 499-525.

BAI, Y.S., LI, L., NIU, Z.J. & CUI, J.L. (2005) Characteristics and Tectonic Setting of Erlongba Formation Volcanic Rocks in Geladandong Area of Central

Qiangtang. Acta Geosicientia Sinica, 26, 113-120 (in Chinese with English abstract).

BERNET, M., ZATTIN, M., GARVER, J.I., BRANDON, M.T. & VANCE, J.A. (2001) Steady-State Exhumation of the European Alps. Geology, 29, 35-38.

BERTRAM, G.T. & MILTON, N.J. (1988) Reconstructing Basin Evolution from Sedimentary Thickness; the Importance of Palaeobathymetric Control, with Reference to the North Sea. *Basin Research*, 1, 247-257.

BLISNIUK, P.M., HACKER, B.R., GLODNY, J., RATSCHBACHER, L., BI, S., WU, Z., MCWILLIAMS, M.O. & CALVERT, A. (2001) Normal Faulting in Central Tibet since at Least 13.5 Myr Ago. *Nature*, 412, 628.

BOND, G.C. & KOMINZ, M.A. (1984) Construction of Tectonic Subsidence Curves for the Early Paleozoic Miogeocline, Southern Canadian Rocky Mountains: Implications for Subsidence Mechanisms, Age of Breakup, and Crustal Thinning. *Geol. Soc. Am. Bull.*, 95, 155-173.

BRUNET, M.F., KOROTAEV, M.V., ERSHOV, A.V. & NIKISHIN, A.M. (2003) The South Caspian Basin: A Review of Its Evolution from Subsidence Modelling. Sedimentary Geology, 156, 119-148.

BUSBY, C.J. & INGERSOLL, R.V. (1995) Tectonics of Sedimentary Basins. Blackwell Science, Cambridge.

CARRAPA, B. & GARCIA-GASTELLANOS, D. (2005) Western Alpine Back-Thrusting as Subsidence Mechanism in the Western Po Basin. Tectonophysics, 406, 197-212.

CEDERBOM, C.E., SINCLAIR, H.D., SCHLUNEGGER, F. & RAHN, M.K. (2004) Climate-Induced Rebound and Exhumation of the European Alps. Geology, 32, 709-712.

CHANG, E.Z. (2000) Geology and Tectonics of the Songpan-Ganzi Fold Belt, Southwestern China. *Int Geol Rev*, 42, 813-831.

CHEN, J.L., WU, J.B., XU, J.F., DONG, Y.H., WANG, B.D. & KANG, Z.Q. (2013) Geochemistry of Eocene High-Mg# Adakitic Rocks in the Northern Qiangtang Terrane, Central Tibet: Implications for Early Uplift of the Plateau. *Geol. Soc. Am. Bull.*, 125, 1800-1819.

CHEN, L., JENKYNS, H.C., XU, G., MATTIOLI, E., DA, X., YI, H., XIA, M., ZHU, Z. & HUANG, Z. (2016) Preliminary Nannofossil and Geochemical Data from Jurassic Black Shales from the Qiangtang Basin, Northern Tibet. *J. Asian Earth Sci.*, 115, 257-267.

CHEN, L., XU, G.W., DA, X.J., JI, C.J. & YI, H.S. (2014) Biomarkers of Middle to Late Jurassic Marine Sediments from a Canonical Section: New Records from the Yanshiping Area, Northern Tibet. *Mar Petrol Geol*, 51, 256-267.

CHEN, S.S., FAN, W.M., SHI, R.D., GONG, X.H. & WU, K. (2017a) Removal of Deep Lithosphere in Ancient Continental Collisional Orogens: A Case Study from Central Tibet, China. *Geochemistry, Geophysics, Geosystems*, 18, 1225-1243.

CHEN, W., ZHANG, S., DING, J., ZHANG, J., ZHAO, X., ZHU, L., YANG, W., YANG, T., LI, H. & WU, H. (2017b) Combined Paleomagnetic and

Geochronological Study on Cretaceous Strata of the Qiangtang Terrane, Central Tibet. *Gondwana Research*, 41, 373-389.

CHENG, L., WANG, J., WAN, Y., FU, X. & ZHONG, L. (2017) Astrochronology of the Middle Jurassic Buqu Formation (Tibet, China) and Its Implications for the Bathonian Time Scale. *Palaeogeography, Palaeoclimatology, Palaeoecology*, 487, 51-58.

CHRISTIE-BLICK, N. & BIDDLE, K.T. (1985) Deformation and Basin Formation Along Strike-Slip Faults. In: Strike-Slip Deformation, Basin Formation, and Sedimentation (Ed. by K. T. Biddle & N. Christie-Blick), 1-34. Society of Economic Paleontologists and Mineralogists, Tulsa, OK, USA.

DAI, J., WANG, C., HéBERT, R., LI, Y., ZHONG, H., GUILLAUME, R., BEZARD, R. & WEI, Y. (2011) Late Devonian Oib Alkaline Gabbro in the Yarlung Zangbo Suture Zone: Remnants of the Paleo-Tethys? *Gondwana Research*, 19, 232-243.

DAN, W., WANG, Q., WHITE, W.M., ZHANG, X.-Z., TANG, G.-J., JIANG, Z.-Q., HAO, L.-L. & OU, Q. (2018) Rapid Formation of Eclogites During a Nearly Closed Ocean: Revisiting the Pianshishan Eclogite in Qiangtang, Central Tibetan Plateau. Chem. Geol., 477, 112-122.

DECELLES, P.G. & GILES, K.A. (1996) Foreland Basin Systems. *Basin research*, 8, 105-123.

DEWEY, J.F., SHACKLETON, R.M., CHENGFA, C. & YIYIN, S. (1988) The Tectonic Evolution of the Tibetan Plateau. Philosophical Transactions of the

Royal Society of London A: Mathematical, Physical and Engineering Sciences, 327, 379-413.

DING, L., XU, Q., YUE, Y., WANG, H., CAI, F. & LI, S. (2014) The Andean-Type Gangdese Mountains: Paleoelevation Record from the Paleocene–Eocene Linzhou Basin. *Earth Planet. Sci. Lett.*, 392, 250-264.

DING, L., YANG, D., CAI, F.L., PULLEN, A., KAPP, P., GEHRELS, G.E., ZHANG, L.Y., ZHANG, Q.H., LAI, Q.Z., YUE, Y.H. & SHI, R.D. (2013a) Provenance Analysis of the Mesozoic Hoh-Xil-Songpan-Ganzi Turbidites in Northern Tibet: Implications for the Tectonic Evolution of the Eastern Paleo-Tethys Ocean. *Tectonics*, 32, 34-48.

DING, W.L., WAN, H., ZHANG, Y.Q. & HAN, G.Z. (2013b) Characteristics of the Middle Jurassic Marine Source Rocks and Prediction of Favorable Source Rock Kitchens in the Qiangtang Basin of Tibet. *J. Asian Earth Sci.*, 66, 63-72.

DONELICK, R.A., O'SULLIVAN, P.B. & KETCHAM, R.A. (2005) Apatite Fission-Track Analysis. Low-Temperature Thermochronology: Techniques, Interpretations, and Applications, 58, 49-94.

DRESSEL, I., SCHECK-WENDEROTH, M. & CACACE, M. (2017) Backward Modelling of the Subsidence Evolution of the Colorado Basin, Offshore Argentina and Its Relation to the Evolution of the Conjugate Orange Basin, Offshore Sw Africa. Tectonophysics, 716, 168-181.

DUNKL, I. (2002) Trackkey: A Windows Program for Calculation and Graphical Presentation of Fission Track Data. Comput Geosci-Uk, 28, 3-12.

EINSELE, G. (1992) Sedimentary Basins: Evolution, Facies, and Sediment Budget. Springer-Verlag, Berlin.

FAN, J.J., LI, C., LIU, Y.M. & XU, J.X. (2015) Age and Nature of the Late Early Cretaceous Zhaga Formation, Northern Tibet: Constraints on When the Bangong-Nujiang Neo-Tethys Ocean Closed. *Int Geol Rev*, 57, 342-353.

FAN, J.J., LI, C., WU, H., ZHANG, T.Y., WANG, M., CHEN, J.W. & XU, J.X. (2016) Late Jurassic Adakitic Granodiorite in the Dong Co Area, Northern Tibet: Implications for Subduction of the Bangong–Nujiang Oceanic Lithosphere and Related Accretion of the Southern Qiangtang Terrane. *Tectonophysics*, 691, Part B, 345-361.

FANG, X., SONG, C., YAN, M., ZAN, J., LIU, C., SHA, J., ZHANG, W., ZENG, Y., WU, S. & ZHANG, D. (2016) Mesozoic Litho- and Magneto-Stratigraphic Evidence from the Central Tibetan Plateau for Megamonsoon Evolution and Potential Evaporites. Gondwana Research, 37, 110-129.

FU, X.G., WANG, J., TAN, F.W., CHEN, M. & CHEN, W.B. (2010) The Late Triassic Rift-Related Volcanic Rocks from Eastern Qiangtang, Northern Tibet (China): Age and Tectonic Implications. *Gondwana Research*, 17, 135-144.

FU, X.G., WANG, J., WANG, Z.J. & CHEN, W.X. (2007) Identification of Sedimentary Gap between the Late Triassic Nadi Kangri Formation and Its Underlying Strata in the Qiangtang Basin, Northern Tibet and Its Geological Significance. *Geological Review*, 53, 329-336 (in Chinese with English abstract).

GALBRAITH, R. (1981) On Statistical Models for Fission Track Counts.

Mathematical Geology, 13, 471-478.

GALBRAITH, R.F. (2005) Statistics for Fission Track Analysis. CRC Press.

GALBRAITH, R.F. & GREEN, P.F. (1990) Estimating the Component Ages in a Finite Mixture. Nucl Tracks Rad Meas, 17, 197-206.

GLEADOW, A. (1981) Fission-Track Dating Methods: What Are the Real Alternatives? Nuclear Tracks, 5, 3-14.

GREEN, P. (1981) A New Look at Statistics in Fission-Track Dating. Nuclear tracks, 5, 77-86.

GRADSTEIN, F.M., OGG, J.G., SMITH, A.G., BLEEKER, W. & LOURENS, L.J. (2004) A New Geologic Time Scale, with Special Reference to Precambrian and Neogene. *Episodes*, 27, 83-100.

GUYNN, J.H., KAPP, P., PULLEN, A., HEIZLER, M., GEHRELS, G. & DING, L. (2006) Tibetan Basement Rocks near Amdo Reveal "Missing" Mesozoic Tectonism Along the Bangong Suture, Central Tibet. *Geology*, 34, 505-508.

HE, J.L., WANG, J., TAN, F.W., CHEN, M., LI, Z.X., SUN, T., WANG, P.K., DU, B.W. & CHEN, W.B. (2014) A Comparative Study between Present and Palaeo-Heat Flow in the Qiangtang Basin, Northern Tibet, China. Marine and Petroleum Geology, 57, 345-358.

HOLT, P.J., ALLEN, M.B. & VAN HUNEN, J. (2015) Basin Formation by Thermal Subsidence of Accretionary Orogens. *Tectonophysics*, 639, 132-143.

HOLT, P.J., ALLEN, M.B., VAN HUNEN, J. & BJøRNSETH, H.M. (2010) Lithospheric Cooling and Thickening as a Basin Forming Mechanism.

859 *Tectonophysics*, 495, 184-194.

860 HOMEWOOD, P., ALLEN, P.A. & WILLIAMS, G.D. (1986) Dynamics of the
861 Molasse Basin of Western Switzerland. In: Foreland Basins (Ed. by P. A. Allen
862 & P. Homewood), 199-217. Special Publication of the International Association
863 of Sedimentologists, Blackwell Science, Oxford.

864 HORTON, B.K. (2012) Cenozoic Evolution of Hinterland Basins in the Andes and
865 Tibet. In: Tectonics of Sedimentary Basins: Recent Advances (Ed. by C. Busby
866 & A. Azor), 427-444. John Wiley & Sons, Ltd.

867 HORTON, B.K. (2018) Sedimentary Record of Andean Mountain Building.
868 Earth-Science Reviews, 178, 279-309.

869 HUANG, Q.T., LIU, W.L., XIA, B., CAI, Z.R., CHEN, W.Y., LI, J.F. & YIN, Z.X.
870 (2017) Petrogenesis of the Majiari Ophiolite (Western Tibet, China):
871 Implications for Intra-Oceanic Subduction in the Bangong–Nujiang Tethys. *J.*
872 *Asian Earth Sci.*, 146, 337-351.

873 HURFORD, A.J. & GREEN, P.F. (1983) The Zeta-Age Calibration of Fission-Track
874 Dating. Isot Geosci, 1, 285-317.

875 JORDAN, T.E. (1981) Thrust Loads and Foreland Basin Evolution, Cretaceous,
876 Western United States. *AAPG bulletin*, 65, 2506-2520.

877 KAPP, P., DECELLES, P.G., GEHRELS, G.E., HEIZLER, M. & DING, L. (2007)
878 Geological Records of the Lhasa-Qiangtang and Indo-Asian Collisions in the
879 Nima Area of Central Tibet. *Geol. Soc. Am. Bull.*, 119, 917-933.

880 KAPP, P., YIN, A., HARRISON, T.M. & DING, L. (2005) Cretaceous-Tertiary

Shortening, Basin Development, and Volcanism in Central Tibet. *Geol. Soc. Am. Bull.*, 117, 865-878.

KAPP, P., YIN, A., MANNING, C.E., HARRISON, T.M., TAYLOR, M.H. & DING, L. (2003) Tectonic Evolution of the Early Mesozoic Blueschist-Bearing Qiangtang Metamorphic Belt, Central Tibet. *Tectonics*, 22.

KAPP, P., YIN, A., MANNING, C.E., MURPHY, M., HARRISON, T.M., SPURLIN, M., LIN, D., DENG, X.G. & WU, C.M. (2000) Blueschist-Bearing Metamorphic Core Complexes in the Qiangtang Block Reveal Deep Crustal Structure of Northern Tibet. *Geology*, 28, 19-22.

KETCHAM, R.A. (2005) The Role of Crystallographic Angle in Characterizing and Modeling Apatite Fission-Track Length Data. Radiation Measurements, 39, 595-601.

KETCHAM, R.A., CARTER, A., DONELICK, R.A., BARBARAND, J. & HURFORD, A.J. (2007) Improved Modeling of Fission-Track Annealing in Apatite. American Mineralogist. 92, 799-810.

KETCHAM, R.A., DONELICK, R.A. & CARLSON, W.D. (1999) Variability of Apatite Fission-Track Annealing Kinetics: Iii. Extrapolation to Geological Time Scales. Am Mineral, 84, 1235-1255.

KNELLER, B.C. (1991) A Foreland Basin on the Southern Margin of Iapetus. *Journal of the Geological Society*, 148, 207-210.

KUHN, P.P., ECHTLER, H., LITTKE, R. & ALFARO, G. (2010) Thermal Basin Modelling of the Arauco Forearc Basin, South Central Chile—Heat Flow and

903 Active Margin Tectonics. *Tectonophysics*, 495, 111-128.

904 LI, C., CHENG, L., HU, K., YANG, Z. & HONG, Y. (1995) Study on the 905 Paleo-Tethys Suture Zone of Lungmu Co-Shuanghu, Tibet. Geological 906 Publishing House, Beijing.

907 LI, G.M., LI, J.X., ZHAO, J.X., QIN, K.Z., CAO, M.J. & EVANS, N.J. (2015a) 908 Petrogenesis and Tectonic Setting of Triassic Granitoids in the Qiangtang 909 Terrane, Central Tibet: Evidence from U-Pb Ages, Petrochemistry and Sr-Nd-Hf 910 Isotopes. *J. Asian Earth Sci.*, 105, 443-455.

911 LI, G.M., QIN, K.Z., LI, J.X., EVANS, N.J., ZHAO, J.X., CAO, M.J. & ZHANG, 912 X.N. (2017a) Cretaceous Magmatism and Metallogeny in the Bangong–Nujiang 913 Metallogenic Belt, Central Tibet: Evidence from Petrogeochemistry, Zircon 914 U–Pb Ages, and Hf–O Isotopic Compositions. *Gondwana Research*, 41, 915 110-127.

916 LI, H.Q., XU, Z.Q., WEBB, A.A.G., LI, T.F., MA, S.W. & HUANG, X.M. (2017c) 917 Early Jurassic Tectonism Occurred within the Basu Metamorphic Complex, 918 Eastern Central Tibet: Implications for an Archipelago-Accretion Orogenic 919 Model. Tectonophysics, 702, 29-41.

920 LI, J. & BATTEN, D.J. (2004) Early Cretaceous Palynofloras from the Tanggula 921 Mountains of the Northern Qinghai-Xizang (Tibet) Plateau, China. Cretaceous 922 Research, 25, 531-542.

923 LI, S., DING, L., GUILMETTE, C., FU, J., XU, Q., YUE, Y. & HENRIQUE-PINTO, 924 R. (2017b) The Subduction-Accretion History of the Bangong-Nujiang Ocean:

Constraints from Provenance and Geochronology of the Mesozoic Strata near Gaize, Central Tibet. *Tectonophysics*, 702, 42-60.

LI, Y., HE, J., HAN, Z., WANG, C., MA, P., ZHOU, A., LIU, S.-A. & XU, M. (2016) Late Jurassic Sodium-Rich Adakitic Intrusive Rocks in the Southern Qiangtang Terrane, Central Tibet, and Their Implications for the Bangong–Nujiang Ocean Subduction. *Lithos*, 245, 34-46.

LI, Y., HE, J., WANG, C., HAN, Z., MA, P., XU, M. & DU, K. (2015c) Cretaceous Volcanic Rocks in South Qiangtang Terrane: Products of Northward Subduction of the Bangong-Nujiang Ocean? *J. Asian Earth Sci.*, 104, 69-83.

LI, Y., HE, J., WANG, C., SANTOSH, M., DAI, J., ZHANG, Y., WEI, Y. & WANG, J. (2013) Late Cretaceous K-Rich Magmatism in Central Tibet: Evidence for Early Elevation of the Tibetan Plateau? *Lithos*, 160, 1-13.

LI, Y., WANG, C., DAI, J., XU, G., HOU, Y. & LI, X. (2015b) Propagation of the Deformation and Growth of the Tibetan–Himalayan Orogen: A Review. *Earth-Science Reviews*, 143, 36-61.

LI, Y., WANG, C. & YI, H. (2002) Filled Sequence and Evolution of the Mesozoic Qiangtang Composite Foreland Basin in the Qinghai-Tibet Plateau. *Journal of Stratigraphy*, 26, 62-67 (in Chinese with English abstract).

LI, Y., WANG, C. & YI, H. (2003) The Late Triassic Collision and Sedimentary Responses at Western Segment of Jinshajing Suture, Tibet. *Acta sedimentologica sinica*, 21, 191-197 (in Chinese with English abstract).

LI, Y., WANG, C., YI, H., SHI, H., LIN, J., ZHU, L. & LI, X. (2001) Fill Models of in the Qiangtang Composite Foreland Basin in Qinghai-Xizang Plateau, China. *Acta Sedimentologica Sinica*, 19, 20-27 (in Chinese with English abstract).

LIANG, X., WANG, G., YANG, B., RAN, H., ZHENG, Y., DU, J. & LI, L. (2017) Stepwise Exhumation of the Triassic Lanling High-Pressure Metamorphic Belt in Central Qiangtang, Tibet: Insights from a Coupled Study of Metamorphism, Deformation and Geochronology. *Tectonics*, 36, 652-670.

LIU, D., SHI, R., DING, L., HUANG, Q., ZHANG, X., YUE, Y. & ZHANG, L. (2017) Zircon U–Pb Age and Hf Isotopic Compositions of Mesozoic Granitoids in Southern Qiangtang, Tibet: Implications for the Subduction of the Bangong–Nujiang Tethyan Ocean. *Gondwana Research*, 41, 157-172.

LIU, Y., SANTOSH, M., ZHAO, Z.B., NIU, W.C. & WANG, G.H. (2011) Evidence for Palaeo-Tethyan Oceanic Subduction within Central Qiangtang, Northern Tibet. *Lithos*, 127, 39-53.

LU, L., ZHANG, K. J., YAN, L. L., JIN, X. & ZHANG, Y. X. (2017) Was Late Triassic Tanggula Granitoid (Central Tibet, Western China) a Product of Melting of Underthrust Songpan-Ganzi Flysch Sediments? *Tectonics*, 36, 902-928.

MAGOON, L.B. & DOW, W.G. (1994) The Petroleum System. In: The Petroleum System: From Source to Trap (Ed. by L. B. Magoon & W. G. Dow), 60, 3-24. American Association of Petroleum Geologists Memoir.

MIALL, A. (1995) Collision-Related Foreland Basins. In: Tectonics of Sedimentary Basins (Ed. by C. J. Busby & R. V. Ingersoll), 393-424. Blackwell Science, Oxford, UK.

969 MILLER, K.G., KOMINZ, M.A., BROWNING, J.V., WRIGHT, J.D., MOUNTAIN, G.S., KATZ, M.E., SUGARMAN, P.J., CRAMER, B.S., CHRISTIE-BLICK, N. & PEKAR, S.F. (2005) The Phanerozoic Record of Global Sea-Level Change. *Science*, 310, 1293-1298.

973 MITROVICA, J.X., BEAUMONT, C. & JARVIS, G.T. (1989) Tilting of Continental Interiors by the Dynamical Effects of Subduction. Tectonics, 8, 1079-1094.

975 MURPHY, M.A., YIN, A., HARRISON, T.M., DüRR, S.B., CHEN, Z., RYERSON, F.J., KIDD, W.S.F., WANG, X. & ZHOU, X. (1997) Did the Indo-Asian Collision Alone Create the Tibetan Plateau? *Geology*, 25, 719-722.

978 NAESER, N.D., NAESER, C.W. & MCCULLOH, T.H. (1989) The Application of Fission-Track Dating to the Depositional and Thermal History of Rocks in Sedimentary Basins. In: Thermal History of Sedimentary Basins (Ed. by N. Naeser & T. Mcculloh), 157-180. Springer.

982 NAYLOR, M. & SINCLAIR, H.D. (2008) Pro- Vs. Retro-Foreland Basins. *Basin Research*, 20, 285-303.

984 NIE, S., YIN, A., ROWLEY, D.B. & JIN, Y. (1994) Exhumation of the Dabie Shan Ultra-High-Pressure Rocks and Accumulation of the Songpan-Ganzi Flysch Sequence, Central China. *Geology*, 22, 999-1002.

987 OGG, J.G., OGG, G. & GRADSTEIN, F.M. (2008) The Concise Geologic Time Scale. Cambridge University Press.

989 O'SULLIVAN, P.B. & PARRISH, R.R. (1995) The Importance of Apatite Composition and Single-Grain Ages When Interpreting Fission-Track Data from

Plutonic Rocks-a Case-Study from the Coast Ranges, British-Columbia. Earth Planet. Sci. Lett., 132, 213-224.

OU, Q., WANG, Q., WYMAN, D.A., ZHANG, H.X., YANG, J.H., ZENG, J.P., HAO, L.L., CHEN, Y.W., LIANG, H. & QI, Y. (2017) Eocene Adakitic Porphyries in the Central - Northern Qiangtang Block, Central Tibet: Partial Melting of Thickened Lower Crust and Implications for Initial Surface Uplifting of the Plateau. *Journal of Geophysical Research: Solid Earth*, 122, 1025-1053.

PEARCE, J.A. & HOUJUN, M. (1988) Volcanic Rocks of the 1985 Tibet Geotraverse: Lhasa to Golmud. Philosophical Transactions of the Royal Society of London A: Mathematical, Physical and Engineering Sciences, 327, 169-201.

PERSANO, C., STUART, F.M., BISHOP, P. & DEMPSTER, T.J. (2005) Deciphering Continental Breakup in Eastern Australia Using Low-Temperature Thermochronometers. Journal of Geophysical Research: Solid Earth, 110.

PULLEN, A. & KAPP, P. (2014) Mesozoic Tectonic History and Lithospheric Structure of the Qiangtang Terrane: Insights from the Qiangtang Metamorphic Belt, Central Tibet. Geological Society of America Special Papers, 507.

PULLEN, A., KAPP, P., GEHRELS, G.E., VERVOORT, J.D. & DING, L. (2008) Triassic Continental Subduction in Central Tibet and Mediterranean-Style Closure of the Paleo-Tethys Ocean. Geology, 36, 351-354.

REINERS, P.W. & BRANDON, M.T. (2006) Using Thermochronology to Understand Orogenic Erosion. Annu. Rev. Earth Planet. Sci., 34, 419-466.

REN, Z.L., CUI, J.P., LIU, C.Y., LI, T.J., CHEN, G., DOU, S., TIAN, T. & LUO, Y.T. (2015) Apatite Fission Track Evidence of Uplift Cooling in the Qiangtang Basin and Constraints on the Tibetan Plateau Uplift. *Acta Geol Sin-Engl*, 89, 467-484.

ROGER, F., JOLIVET, M., CATTIN, R. & MALAVIEILLE, J. (2011) Mesozoic-Cenozoic Tectonothermal Evolution of the Eastern Part of the Tibetan Plateau (Songpan-Garzê, Longmen Shan Area): Insights from Thermochronological Data and Simple Thermal Modelling. Geological Society, London, Special Publications, 353, 9-25.

ROHRMANN, A., KAPP, P., CARRAPA, B., REINERS, P.W., GUYNN, J., DING, L. & HEIZLER, M. (2012) Thermochronologic Evidence for Plateau Formation in Central Tibet by 45 Ma. *Geology*, 40, 187-190.

ROWLEY, D.B. & CURRIE, B.S. (2006) Palaeo-Altimetry of the Late Eocene to Miocene Lunpola Basin, Central Tibet. *Nature*, 439, 677-681.

ROYDEN, L. & KEEN, C.E. (1980) Rifting Process and Thermal Evolution of the Continental Margin of Eastern Canada Determined from Subsidence Curves. *Earth Planet. Sci. Lett.*, 51, 343-361.

SACHSENHOFER, R.F., LANKREIJER, A., CLOETINGH, S. & EBNER, F. (1997) Subsidence Analysis and Quantitative Basin Modelling in the Styrian Basin (Pannonian Basin System, Austria). *Tectonophysics*, 272, 175-196.

SCIUNNACH, D. & GARZANTI, E. (2012) Subsidence History of the Tethys Himalaya. *Earth-Science Reviews*, 111, 179-198.

SCLATER, J.G. & CHRISTIE, P.A.F. (1980) Continental Stretching: An Explanation of the Post-Mid-Cretaceous Subsidence of the Central North Sea Basin. *Journal of Geophysical Research: Solid Earth*, 85, 3711-3739.

SILVIA, O.S., RAMON, S., JOAN, G., ROBERT, O., RAMON, M., JOSé, A., ISABEL, S.R. & LUIS, M. (2017) Subsidence and Thermal History of an Inverted Late Jurassic-Early Cretaceous Extensional Basin (Cameros, North-Central Spain) Affected by Very Low- to Low-Grade Metamorphism. Basin Research, 29, 156-174.

SINCLAIR, H.D. & NAYLOR, M. (2012) Foreland Basin Subsidence Driven by Topographic Growth Versus Plate Subduction. *Geol. Soc. Am. Bull.*, 124, 368-379.

SOBEL, E.R. & SEWARD, D. (2010) Influence of Etching Conditions on Apatite Fission-Track Etch Pit Diameter. Chem. Geol., 271, 59-69.

SONG, C., ZENG, Y., YAN, M., FANG, X., FENG, Y., PAN, J., LIU, X., MENG, Q., HU, C. & ZHONG, S. (2017) Sedimentary Conditions of Evaporites in the Late Jurassic Xiali Formation, Qiangtang Basin: Evidence from Geochemistry Records. *Acta Geologica Sinica - English Edition*, 91, 156-174.

SONG, C.Y. (2012) Evolution of Mesozoic Sedimentary Basin in Qiangtang and Its Significance in Petroleum Geology, Chinese Academy of Geological Sciences, Beijing (in Chinese with English abstract).

SONG, P., DING, L., LI, Z., LIPPERT, P.C. & YUE, Y. (2017) An Early Bird from Gondwana: Paleomagnetism of Lower Permian Lavas from Northern Qiangtang (Tibet) and the Geography of the Paleo-Tethys. Earth and Planetary Science

Letters, 475, 119-133.

STAPEL, G., CLOETINGH, S. & PRONK, B. (1996) Quantitative Subsidence Analysis of the Mesozoic Evolution of the Lusitanian Basin (Western Iberian Margin). *Tectonophysics*, 266, 493-507.

STECKLER, M.S. & WATTS, A.B. (1978) Subsidence of the Atlantic-Type Continental Margin Off New York. *Earth Planet. Sci. Lett.*, 41, 1-13.

TANG, M., LIU-ZENG, J., HOKE, G.D., XU, Q., WANG, W., LI, Z., ZHANG, J. & WANG, W. (2017) Paleoelevation Reconstruction of the Paleocene-Eocene Gonjo Basin, Se-Central Tibet. *Tectonophysics*, 712–713, 170-181.

TIAN, Y., KOHN, B.P., HU, S. & GLEADOW, A.J.W. (2014) Postorogenic Rigid Behavior of the Eastern Songpan-Ganze Terrane: Insights from Low-Temperature Thermochronology and Implications for Intracontinental Deformation in Central Asia. *Geochemistry, Geophysics, Geosystems*, 15, 453-474.

TOZER, B., WATTS, A.B. & DALY, M.C. (2017) Crustal Structure, Gravity Anomalies, and Subsidence History of the Parnaíba Cratonic Basin, Northeast Brazil. Journal of Geophysical Research: Solid Earth, 122, 5591-5621.

U.S. GEOLOGICAL SURVEY (2006) FGDC Digital Cartographic Standard for Geologic Map Symbolization (Postscript Implementation). U.S. Geological Survey Techniques and Methods 11-A2. http://pubs.usgs.gov/tm/2006/11A02/

VERGéS, J., MARZO, M., SANTAEULàRIA, T., SERRA-KIEL, J., BURBANK, D.W., MUñOZ, J.A. & GIMéNEZ-MONTSANT, J. (1998) Quantified Vertical

Motions and Tectonic Evolution of the Se Pyrenean Foreland Basin. In: Cenozoic Foreland Basins of Western Europe (Ed. by A. Mascle, C. Puigdefàbregas, H. P. Luterbacher & M. Fernàndez), 134, 107-134. Special Publications, Geological Society of London.

VERMEESCH, P. (2012) On the Visualisation of Detrital Age Distributions. Chem. Geol., 312-313, 190-194.

WANG, C., DAI, J., ZHAO, X., LI, Y., GRAHAM, S.A., HE, D., RAN, B. & MENG, J. (2014) Outward-Growth of the Tibetan Plateau During the Cenozoic: A Review. *Tectonophysics*, 621, 1-43.

WANG, C., YIN, H., LI, Y., DENG, B., LIU, D., WANG, G., SHI, H., LI, Y., MA, R. & LIN, J. (2001) The Geological Evolution and Prospective Oil and Gas Assessment of the Qiangtang Basin in Northern Tibetan Plateau. Geological Publishing House, Beijing.

WANG, C.S., ZHAO, X.X., LIU, Z.F., LIPPERT, P.C., GRAHAM, S.A., COE, R.S., YI, H.S., ZHU, L.D., LIU, S. & LI, Y.L. (2008b) Constraints on the Early Uplift History of the Tibetan Plateau. *Proc. Natl. Acad. Sci. U. S. A.*, 105, 4987-4992.

WANG, J., FU, X., CHEN, W. & WANG, Z. (2007) The Late Triassic Paleo-Weathering Crust in the Qiangtang Basin, Northern Tibet: Geology, Geochemistry and Significance. *Acta Sedimentologica Sinica*, 25, 487 (in Chinese with English abstract).

WANG, J., FU, X.G., CHEN, W.X., WANG, Z.J., TAN, F.W., CHEN, M. & ZHUO, J.W. (2008a) Chronology and Geochemistry of the Volcanic Rocks in Woruo

Mountain Region, Northern Qiangtang Depression: Implications to the Late Triassic Volcanic-Sedimentary Events. *Sci. China Ser. D-Earth Sci.*, 51, 194-205.

WANG, J., TAN, F., LI, Y., LI, Y., CHEN, M., WANG, C., GUO, Z., WANG, X., DU, B. & ZHU, Z. (2004b) The Potential of the Oil and Gas Resources in Major Sedimentary Basins on the Qinghai-Xizang Plateau. Geological Publishing House, Beijing.

WANG, J., TAN, F., WANG, X., DU, B. & CHEN, M. (2004a) The Sedimentary and Tectonic Characteristics of Qiangtang Basin in the Early Jurassic in Northern Xizang (Tibet). *Acta Sedimentologica Sinica*, 22, 198-205 (in Chinese with English abstract).

WANG, L.B., ZHANG, Y.Q., CAI, J.J. & HAN, G.Z. (2013) Characteristics of the Upper Jurassic Marine Source Rocks and Prediction of Favorable Source Rock Kitchens in the Qiangtang Basin, Tibet. *J Earth Sci-China*, 24, 815-829.

WANG, L.C. & WEI, Y.S. (2013) Apatite Fission Track Thermochronology Evidence for the Mid-Cretaceous Tectonic Event in the Qiangtang Basin, Tibet. Acta Petrologica Sinica, 29, 1039-1047 (in Chinese with English abstract).

WANG, Q., WYMAN, D.A., LI, Z.X., SUN, W., CHUNG, S.L., VASCONCELOS, P.M., ZHANG, Q., DONG, H., YU, Y. & PEARSON, N. (2010) Eocene North–South Trending Dikes in Central Tibet: New Constraints on the Timing of East–West Extension with Implications for Early Plateau Uplift? *Earth Planet. Sci. Lett.*, 298, 205-216.

WANG, Z., WANG, J., FU, X., FENG, X., WANG, D., SONG, C., CHEN, W., ZENG, S. & YU, F. (2017b) Provenance and Tectonic Setting of the Quemoco Sandstones in the North Qiangtang Basin, North Tibet: Evidence from Geochemistry and Detrital Zircon Geochronology. *Geological Journal*, https://doi.org/10.1002/gj.2967.

WANG, Z., WANG, J., FU, X., ZHAN, W., YU, F., FENG, X., SONG, C., CHEN, W. & ZENG, S. (2017a) Organic Material Accumulation of Carnian Mudstones in the North Qiangtang Depression, Eastern Tethys: Controlled by the Paleoclimate, Paleoenvironment, and Provenance. *Mar Petrol Geol*, 88, 440-457.

WATTS, A.B. & RYAN, W.B.F. (1976) Flexure of the Lithosphere and Continental Margin Basins. *Tectonophysics*, 36, 25-44.

WATTS, A.B., KARNER, G.D. & STECKLER, M.S. (1982) Lithospheric Flexure and the Evolution of Sedimentary Basins. Philosophical Transactions of the Royal Society of London A: Mathematical, Physical and Engineering Sciences, 305, 249-281.

WEISLOGEL, A.L., GRAHAM, S.A., CHANG, E.Z., WOODEN, J.L., GEHRELS, G.E. & YANG, H. (2006) Detrital Zircon Provenance of the Late Triassic Songpan-Ganzi Complex: Sedimentary Record of Collision of the North and South China Blocks. *Geology*, 34, 97-100.

WU, Z., WU, X., ZHAO, Z., LU, L., YE, P. & ZHANG, Y. (2014) Shrimp U–Pb Isotopic Dating of the Late Cretaceous Volcanic Rocks and Its Chronological Constraint on the Red-Beds in Southern Qiangtang Block. *Acta Geoscientica*

Sinica, 35, 567-572 (in Chinese with English abstract).

XU, Q., DING, L., ZHANG, L.Y., CAI, F.L., LAI, Q.Z., YANG, D. & JING, L.Z. (2013) Paleogene High Elevations in the Qiangtang Terrane, Central Tibetan Plateau. *Earth Planet. Sci. Lett.*, 362, 31-42.

YAO, X., LIU, S., BAI, Y. & JI, H. (2017) Neogene Residual Subsidence and Its Response to a Sinking Slab in the Deep Mantle of Eastern China. *J. Asian Earth Sci.*, 143, 269-282.

YAN, M., ZHANG, D., FANG, X., REN, H., ZHANG, W., ZAN, J., SONG, C. & ZHANG, T. (2016) Paleomagnetic Data Bearing on the Mesozoic Deformation of the Qiangtang Block: Implications for the Evolution of the Paleo-and Meso-Tethys. *Gondwana Research*, 39, 25.

YANG, R., CAO, J., HU, G., BIAN, L., HU, K. & FU, X. (2017) Marine to Brackish Depositional Environments of the Jurassic–Cretaceous Suowa Formation, Qiangtang Basin (Tibet), China. Palaeogeography, Palaeoclimatology, Palaeoecology, 473, 41-56.

YIN, A. & HARRISON, T.M. (2000) Geologic Evolution of the Himalayan-Tibetan Orogen. *Annu. Rev. Earth Planet. Sci.*, 28, 211-280.

YIN, J. (2016) Bathonian–Callovian (Middle Jurassic) Ammonites from Northwestern Qiangtang Block, Tibet, and the Revised Age of the Suowa Formation. *Proceedings of the Geologists' Association*, 127, 245-263.

YIN, J. & CHANDLER, R.B. (2016) Aalenian to Lower Bajocian Ammonites from the Qiangtang Block (North Tibet). *Proceedings of the Geologists' Association*, 127, 170-186.

ZENG, S., HU, X., LI, J., XU, S., FANG, H. & CAI, J. (2015) Detection of the Deep Crustal Structure of the Qiangtang Terrane Using Magnetotelluric Imaging. *Tectonophysics*, 661, 180-189.

ZHAI, Q. & LI, C. (2007) Zircon Shrimp Dating of Volcanic Rock from Nadigangri Formation in Juhuashan, Qiangtang, Northern Tibet and Its Geological Significance. Acta Geologica Sinica, 81, 795-800 (in Chinese with English abstract).

ZHAI, Q.G., JAHN, B.M., SU, L., WANG, J., MO, X.X., LEE, H.Y., WANG, K.L. & TANG, S.H. (2013) Triassic Arc Magmatism in the Qiangtang Area, Northern Tibet: Zircon U-Pb Ages, Geochemical and Sr-Nd-Hf Isotopic Characteristics, and Tectonic Implications. *J. Asian Earth Sci.*, 63, 162-178.

ZHAI, Q.G., JAHN, B.M., WANG, J., HU, P.Y., CHUANG, S.L., LEE, H.Y., TANG, S.H. & TANG, Y. (2015) Oldest Paleo-Tethyan Ophiolitic Mélange in the Tibetan Plateau. *GSA Bulletin*, 128, 355-373.

ZHANG, K.J. (2000) Cretaceous Palaeogeography of Tibet and Adjacent Areas (China): Tectonic Implications. Cretaceous Research, 21, 23-33.

ZHANG, K.J. & TANG, X.C. (2009) Eclogites in the Interior of the Tibetan Plateau and Their Geodynamic Implications. *Chinese Sci Bull*, 54, 2556-2567.

ZHANG, K.J., TANG, X.C., WANG, Y. & ZHANG, Y.X. (2011) Geochronology, Geochemistry, and Nd Isotopes of Early Mesozoic Bimodal Volcanism in Northern Tibet, Western China: Constraints on the Exhumation of the Central

Qiangtang Metamorphic Belt. *Lithos*, 121, 167-175.

ZHANG, K.J., XIA, B.D., WANG, G.M., LI, Y.T. & YE, H.F. (2004) Early Cretaceous Stratigraphy, Depositional Environments, Sandstone Provenance, and Tectonic Setting of Central Tibet, Western China. GSA Bulletin, 116, 1202-1222.

ZHANG, K.J., ZHANG, Y.X., LI, B., ZHU, Y.T. & WEI, R.Z. (2006) The Blueschist-Bearing Qiangtang Metamorphic Belt (Northern Tibet, China) as an in Situ Suture Zone: Evidence from Geochemical Comparison with the Jinsa Suture. *Geology*, 34, 493-496.

ZHANG, K.J., ZHANG, Y.X., TANG, X.C. & XIA, B. (2012) Late Mesozoic Tectonic Evolution and Growth of the Tibetan Plateau Prior to the Indo-Asian Collision. *Earth-Science Reviews*, 114, 236-249.

ZHANG, X.R., SHI, R.D., HUANG, Q.S., LIU, D.L., GONG, X.H., CHEN, S.S., WU, K., YI, G.D., SUN, Y.L. & DING, L. (2014) Early Jurassic High-Pressure Metamorphism of the Amdo Terrane, Tibet: Constraints from Zircon U-Pb Geochronology of Mafic Granulites. Gondwana Research, 26, 975-985.

ZHAO, Z., BONS, P.D., STÜBNER, K., WANG, G.-H. & EHLERS, T.A. (2017) Early Cretaceous Exhumation of the Qiangtang Terrane During Collision with the Lhasa Terrane, Central Tibet. *Terra Nova*, 29, 382-391.

ZHAO, Z.B., BONS, P.D., WANG, G.H., LIU, Y. & ZHENG, Y.L. (2014) Origin and Pre-Cenozoic Evolution of the South Qiangtang Basement, Central Tibet. *Tectonophysics*, 623, 52-66.

ZHAO, Z., BONS, P.D., WANG, G., SOESOO, A. & LIU, Y. (2015) Tectonic Evolution and High-Pressure Rock Exhumation in the Qiangtang Terrane, Central Tibet. *Solid Earth*, 6, 457-473.

ZHU, D.C., LI, S.M., CAWOOD, P.A., WANG, Q., ZHAO, Z.D., LIU, S.A. & WANG, L.Q. (2016) Assembly of the Lhasa and Qiangtang Terranes in Central Tibet by Divergent Double Subduction. *Lithos*, 245, 11.

ZHU, D.C., ZHAO, Z.D., NIU, Y.L., DILEK, Y., HOU, Z.Q. & MO, X.X. (2013) The Origin and Pre-Cenozoic Evolution of the Tibetan Plateau. *Gondwana Research*, 23, 1429-1454.

ZHU, T.X., QIN, J.H., ZHANG, Z.G., WANG, X.L., LUO, J.L. & ZHUANG, Z.H. (1996) The Geological Multi-Engineering of West Qiangtang Basin (Qt96yz-01), Managing Department of Tibet Oil and Gas Exploration Project, CNPC.

ZHU, T.X., YU, Q., YONG, Y.Y., JIA, B.J., QIN, J.H., ZHANG, Z.G., WANG, X.L., TAN, Q.Y., XIE, Y., LI, M.H., LI, Q.X. & FENG, X.C. (1997) The Tibet Petroleumgeological Survey Report (Qz-97-102101), Managing Department of Tibet Oil and Gas Exploration Project, CNPC.

Table 1 Biostratigraphy constrained by bivalves in the Quemo Co section and magnetostratigraphy

Stratigraphy	Bivalves	Biostratigraphy Age	Magnetostratigraphy Age of Fang *et al.* (2016)	Environment
Xueshan Fm.	Assemblage *Radulopecten fibrosus- Gervillella orientalis- Placunopopsis duriuscula* *Meleagrinella nieniexionglaensis* Wen, *Radulopecten fibrosus* (Sowerby), *Miyagipecten lavis* (Wen), *Placunopsis duriuscula* (Phillips), *P*. sp., *Bakevellia* (*Bakevellia*) *waltoni* (Lycett) *Gervillella qinghaiensis* Wen, *G. orientalis* (Douville), *G*. cf. *siliqua* (Eudes-Deslongchangs), *Plagiostoma* cf. *channoni* Cox, *Pseudolimea duplicata* (Sowerby), *Lopha maliensis* Tong, *Modiolus* (*Modiolus*) *imbricatus* Sowerby, *Protocardia qinghaiensis* Wen, *Corbicellopsis laevis* (Sowerby), *Unicardiopsis* cf. *acesta* (d'Orbigny), *Quenstedtia* cf. *oblita* Greppin, *Q*. cf. *dingriensis* Wen, *Mactromya qinghaiensis* Wen, *M. gibbasa* (Morris et Lycett), *Astarte togtonheensis* Wen, *A*. cf. *elegans* Sowerby, *Tancredia triangularis* Wen, *Pseudotrapezium cordiforme* (Deshayes), *Anisocardia* (*Anisocardia*) *togtonheensis* Wen, *A*. (*Antiquicyprina*) cf. *trapezoidalis* Wen, *Pholadomya* cf. *carinata* Goldfuss, *Pleuromya uniformis* (Sowerby), *Playtmyoidea* sp.	Kimmeridgian	<157.5 Ma	Marine
Suowa Fm.	Assemblage *Myopholas multicostata- Placunopsis duriuscula- Camptonectes (Camptonectes) auritus* *Palaeonucula* sp., *Mesosacella morrisi* (Deshayes), *M. wenquanensis* Sha, Fursich, Smith et Wang, *Nuculana* (*Praesacella*) cf. *ovum* (Sowerby), *Grammatodon* (*Grammatodon*) cf. *clathratum* (Leckenby), *Pinna* sp., *Meleagrinella* sp., *Pteria* cf. *plana* (Morris et Lycett), *Miyagipecten laevis* (Wen), *Radulopecten tipperi* Cox, *R. vagans* (Sowerby), *R. tripartitus* Sha, Fursich, Smith et Wang, *R. fibrosus* (Sowerby), *R. pamirensis* Wen, *R. gerzensis* Wen, *Camptonectes* (*Camptonectes*) *auritus* (Schlotheim), *C*. (*C*.) *laminatus* (Sowerby), *C*. (*Camptochlamys*) *clathratus* (Roemer), *C*. (*Annulinectes*) *obscurus* (Sowerby), *Propeamussium* (*Propeamussium*) cf. *pumilum* (Lamarck), *Placunopsis* cf. *subelongata* (d'Orbigny), *Placunopsis* cf. *socialis* Morris et Lycett, *P. duriuscula* (Phillips), *Gervillella qinghaiensis* Wen, *G. siliqua* (Eudes-Deslongchamps), *G*. sp., *Bakevellia*? sp., *Aguilerella* sp., *Pseudolimea duplicata* (Sowerby), *P. tjubegatanica* (Repman), *P*. sp., *Plagiosto-ma* cf. *channoni* Cox, *Lopha* cf. *tifoensis* Cox, *L*. cf. *maliensis* Tong, *Liostrea* cf. *jiangjinensis* Wen, *L*. cf. *birmanica* (Reed), *L*. cf. *blanfordi* Cox, *Plicatula* sp., *Modiolus* (*Modiolus*) *imbricatus* Sowerby, *M*. (*M*.) cf. *trigonus* Chen, *Myophorella*? sp., *Protocardia stricklandi* (Morris et Lycett), *P. qinghaiensis* Wen, *Mactromya* cf. *qinghaieusis* Wen, *Astarte togtonheensis* Wen, *A*. cf. *elegans* Sowerby, *A*. cf. *maliensis* Tong, *Astartoides gambaensis* Wen et Lan, *A*. cf. *dingriensis* Wen, *Anisocardia* (*Anisocardia*) *rostrata* (Sowerby), *A*. (*A*.) cf. *channoni* Cox, *A*. (*A*.) *togtonheensis* Wen, *A*. (*A*.) sp., *A*. (*Anitiquicyprina*) cf. *trapezoidalis* Wen, *Pseudotrapezium cordiforme* (Deshayes), *Amiodon fengdengensis* (Chen), *A*. cf. *khoratensis* (Hayami), *Platymyoidea* sp., *Myopholas multicostata* (Agassiz), *M. percostata* Douville, *Pleuromya* cf. *uniformis* (Sowerby), *P. subelongata* (d'Orbigny), *P*. sp.	Callovian-Oxfordian	160.1-<157.5 Ma	Marine
Xiali Fm.	Assemblage *Pteroperna costatula— Radulopecten vagans* *Palaeonucula* sp., *Pinna*? sp., *Meleagrinella* cf. *braamburiensis* (Phillips), *Radulopecten tipperi* Cox, *R. vagans* (Sowerby), *R. pamirensis* Wen, *R*. sp., *Placuopsis duriuscula* (Phillips), *Bakevillia (Bakevellia) waltoni* (Lycett), *Gervillella qinghaiensis* Wen, *Costigervillia minima* Wen, *Lopha* cf. *tifoensis* Cox, *Liostrea jiangjinensis* Wen, *Pteria plana* Roemer, *Pteroperna costatula* (Deslongchamps), *P*. sp., *Modiolus* (*Modiolus*) *imbricatus* Sowerby, *Vaugonia* cf. *yanshipingensis*	Bathonian-Callovian	163.3-160.1 Ma	Marine

	Wen, *Protocardia* (*P.*) *qinghaiensis* Wen, *P.* (*P.*) *stricklandi* (Morris et Lycett), *Corbicellopsis* cf. *laevis* (Sowerby), *Unicardiopsis amdoensis* Wen, *Corbula yanshipingeusis* Wen, *C. kidugalloensis* Cox, *C.* sp., *Astarte* cf. *elegans* Sowerby, *A.* sp., *Anisocardia* (*Anisocardia*) cf. *channoni* Cox, *A.* (*A.*) *rostrata* (Sowerby), *Pseudotrapezium cordiforme* (Deshayes), *Amiodon* cf. *khoratensis* (Hayami), *Thracia togtonheensis* Wen			
Buqu Fm.	Assemblage *Isognomon (Mytiloperna) bathonicus- Protocardia hepingxiangensis-Praeexogyra cf. acaminata*	Bathonian	165.5-163.3 Ma	Marine
	Liostrea birmanica, *Ceratomya undalat*, *C. concentrica*, *Grammatodon* (*Grammatodon*) *clathratum*, *Pinna tibetica*, *P. nyainrongensis*, *Radulopecten tipperi*, *Protocardia hepingxiangensis*, *Liostrea jiangjinensis*, *L. zadoensis*, *Lopha maliensis*, *L. baqenensis*, *Entolium nieniexionglaensis*, *Praeexogyra* cf. *acaminata*, *Radulopecten shuanghuensis*, *Gervillella qinghaiensis*, *Pteria problematica, Modiolus* (*Modiolus*) *trigonus*, *Mactromya qinghaiensis*, *Neomiodon yanshipingensis*, *A.* (*Antiquicyprina*) *trapezoidalis*, *Pholadomya socialis qinghaiensis*			
Quemocuo Fm.	*Quenstedtia? sp.*	Bajocian	>171.2-165.5 Ma	Marine
	Assemblage *Undulatula perlonga- Psilunio chaoi*			Fresh water
	Psilunio chaoi Grabau, *P. lateriplanus* Ma, *P. thailandicus* (Hayami), *P. sinensis* Gu, *Lamprotula* (*Eolamprotula*) sp., *Undulatula perlonga* Gu, *U. ptychorhyncha* Gu, *Cuniopsis* cf. *johannisbohmi* (Frech), *Solenaia tanggulaensis* Wen, *Unio* cf. *obrustschewi* Martinson, *Margaritifera isfarensis* Chernyshev			
Erlongba Fm.	Assemblage *Amonotis togtonheensis-Cardium (Tulongocardium) xizhangensis*	Norian-Rhaetian	212±1.7 Ma (Volcanics, Bai *et al.*, 2005)	
Bagong Fm.	Assemblage *Halobia superbescens- H. disperseinsecta*	Norian		
	Assemblage *Amonotis togtonheensis-Cardium* (*Tulongocardium*) *xizhangensis*			
Bolila Fm.	*Cassianella cf. berychi, Halobia plicosa, H. superbescens, H. sp., Plagiostoma sp.*	Carnian		

Bivalves are from Geological report of the 1:250, 000 regional geological survey in Chibuzhang Co area.

Table 2 Apatite fission track data for the Qiangtang Basin

Sample	Stratigraphy	ρs [a] (10^5 cm^{-2})	*N*s [b]	ρi [a] (10^5 cm^{-2})	*N*i [b]	ρd [a] (10^5 cm^{-2})	*N*d [b]	$P(\chi^2)$ [c]	*D*par [d] (μm)	[*U*] [e] (ppm)	Central age [f] (Ma)	±1σ	Dis. [g] (%)	*N.* [h]	MTL (μm)	±1σ	*Nc.* [i]
D0609	J_2x	9.418	728	12.903	1152	12.4	8749	1.00	2.65	17.91	113.6	5.4	0	30	12.17	0.36	20
D0815	J_2x	10.0	148	27.365	405	12.3	8749	0.54	2.84	30.46	65.4	6.3	0	9	/	/	/
ED0616	J_2x	5.403	667	10.726	1324	12.0	8749	0.00	2.00	12.15	90.7	6.8	28	27	11.70	0.31	29
ED0620	T_3d	4.468	652	14.281	2084	12.0	8749	0.24	1.98	15.54	55	2.5	4.7	32	11.71	0.56	28
EP1502	J_2x	4.508	702	14.456	2251	12.2	8749	0.00	2.23	16.84	55.6	3.7	25	28	10.84	0.44	29
EP1503	J_2b	4.775	609	19.247	2445	12.1	8749	0.14	2.20	22.7	44.6	2.3	14	30	9.26	0.39	31
EP1504-09	K_2a	5.256	1048	18.776	3744	12.1	8749	0.23	2.55	19.54	49.1	2	10	40	13.4	0.45	15
EP1504-17	K_2a	5.848	576	17.188	1693	12.0	8749	0.03	3.49	18.01	62.5	4.2	17	18	14.54	0.32	5
EP1505	T_3d	7.043	836	23.361	2773	12.2	8749	0.40	2.40	28.59	53.7	2.4	9.2	32	12.87	0.29	22
EP1506	T_3d	9.154	638	19.283	1344	12.2	8749	0.93	2.48	22.32	84.1	4	0	30	13.75	0.48	17

PQ1503	J_2q	4.492	549	15.921	1946	11.3	6621	0.00	1.74	17.11	40.1	2.6	23	30	12.59	0.14	101
PQ1506	J_2x	9.082	801	12.492	1190	12.4	8749	100	2.15	16.52	120.9	5.5	0	32	12.01	0.22	37

[a] ρs, ρi, ρd are track densities of spontaneous, induced and dosimeter tracks.

[b] Ns, Ni, Nd are the number of spontaneous, induced and dosimeter tracks.

[c] P(χ2) is the value of chi-square test (Galbraith, 1981; Green, 1981).

[d] *D*par is the etch pit diameter, which is used as a proxy for the influence of chemical composition on track annealing (Donelick *et al.*, 2005).

[e] Uranium content calculated with TrackKey (Dunkl, 2002).

[f] Central ages are calculated using TrackKey (Dunkl, 2002) with 1σ standard error. Ages are calculated with a ζ=292.4±17.9 for a standard IRMM540 glass.

[g] Dispersion is the standard deviation of the true single-grain ages as a percentage of their central age (Galbraith, 2005).

[h] N. is the number of grains counted for age calculation.

[i] Nc. is the number of measured horizontal confined tracks.

Figure legends:

Fig. 1. a, Major terranes and sutures of the Tibetan plateau. b, Geological map of Qiangtang basin and adjacent terranes (modified after Kapp *et al.*, 2005). WK-ATSZ = West Kunlun-Altyn Tagh suture zone; SKSZ = South Kunlun suture zone; CQMB = Central Qiangtang metamorphic belt; JRSZ = Jinsha River suture zone; BNSZ = Bangong-Nujiang suture zone. Numbers in grey stars represent the localities of composite sections: 1, Duxue Mt.; 2, Shuangquan Lake; 3, Heihuling; 4, Nadigangri; 5, Changshui River; 6, Amugang; 7, Zuerkenwula Mt.; 8, Dangmagang; 9, Quemo Co; 10, Biluo Co; 11, Dazhuoma.

Fig. 2. Correlation of sequences, lithologies and paleo-environments of main Mesozoic stratigraphic units of the Qiangtang Basin. Not drawn to scale. The lithologies and interpretations of depositional environment of both the North and South Qiangtang are from field observations and geological reports. The age of Nadigangri Fm. comes from Zhai & Li (2007), Wang et al. (2008b) and Fu et al. (2010). Ages of Jurassic sequences are from magnetostratigraphy of Fang et al. (2016). The age of Abushan Fm. is from Li et al. (2015c). The legend of lithology is same to that of Fig. 4. All symbols are filled using patterns provided by U.S. Geological Survey (2006).

Fig. 3. Remote sensing images of specific profiles of continuous successions in Nadigangri (a) and Quemo Co (b) from Google Earth©. Structural dips are labelled

1249 on the strata. The solid lines are boundaries between stratigraphic units. The yellow dashed lines represent unconformities. T_3*nd* = Nadigangri Formation; T_3*b* = Bolila Formation; T_3*bg* = Bagong Formation; T_3*e* = Erlongba Formation; J_2*q* = Quemocuo Formation; J_2*b* = Buqu Formation; J_2*x* = Xiali Formation; J_3*s* = Suowa Formation; J_3*b* = Bailongbinghe Formation; J_3K_1*x* = Xueshan Formation; E_2*k* = Kangtuo Formation.

1255 Fig. 4. Simplified stratigraphic framework of nine composite sections in the North Qiangtang sub-basin. The stratigraphic codes are same to those of Fig. 3. Other codes are: $P_{1\text{-}2}$*l* = Lugu Formation; T_3*j* = Juhuashan Formation; T_3*z* = Zangxiahe Formation; T_3*T* = Tumengela Group; E_2*s* = Suonahu Formation; $E_{1\text{-}2}$*t* = Tuotuohe Formation; E_{2+3}*y* = Yulinshan Formation; N_1*c* = Chabaoma Formation; N_2*q* = Quguo Formation; N_2*sq* = Shuangquanhu Formation.

1262 Fig. 5. Simplified stratigraphic framework of two composite sections in the South Qiangtang sub-basin. The legend, scale and stratigraphic codes are same to those of Fig. 4. Other codes are: T_3*a* = Adula Formation; T_3*d* = Duogaila Formation; T_3*R* = Riganpeicuo Group; T_3J_1*s* = Suobucha Formation; J_1*q* = Quse Formation; J_2*s* = Sewa Formation; K_2*a* = Abushan Formation.

1268 Fig. 6. Decompaction scheme (modified after Allen and Allen, 2005).

1270 Fig. 7. Specific indicators for assessment of paleo-water depth in stratigraphic sections. (a) Oscillatory ripples preserved in the bottom of tidal sandstones (Late Triassic Duogaila Formation, Dazhuoma; paleo-water depth ≈ 50±50 m). (b) Fining-upward sequence with each starting with conglomerate or pebbled sandstones (Middle Jurassic Quemocuo Formation, Amugang; paleo-water depth ≈ 10±10 m). (c) Current bedding limestone (Middle Jurassic Quemocuo Formation, Amugang; paleo-water depth ≈50±50 m). (d) Ripples in tidal sandstones (Middle Jurassic Xiali Formation, Dazhuoma; paleo-water depth ≈50±50 m). (e) Ammonite in mudstone (Late Jurassic Bailongbinghe Formation, Changshui River; paleo-water depth ≈ 50 m). (f) Directional arrangement of gravels in fluvial sandstones (Late Cretaceous Abushan Formation, Biluo Co; paleo-water depth ≈ 10±5 m).

Fig. 8. Subsidence curves for composite sections in Fig. 1. The thick solid line represents backstripped tectonic subsidence. The thin solid line represents total decompacted subsidence. The grey-shade areas represent the first stage of subsidence from Late Triassic to Early Jurassic based on the subsidence histories, combined with previous work on sediment provenance and timing of deformation. The reference lines representing subsidence rate are shown are each of the plots.

Fig. 9. Magnification of the tectonic subsidence histories from 172 to 120 Ma. The reference lines representing subsidence rate are shown are each of the plots. The shaded area represent the gradual cessation of subsidence across the Qiangtang Basin, with the final termination at about 148 Ma. The subsidence curves in the North

Qiangtang are represented by solid lines, while the South Qiangtang are represented by dotted lines.

Fig. 10. Radial plots of detrital apatite fission track ages in the Qiangtang Basin using DensityPlotter (Vermeesch, 2012).

Fig. 11. Weighted mean thermal paths for sandstones in the Qiangtang Basin. The mélange and granite samples are from the Central Uplift studied by Zhao *et al.* (2017). All thermal paths display cooling starting from 150-130 Ma. The depth is calculated by assuming a geothermal gradient of 20 °C/km.

Fig. 12. Schematic map showing the paleo-current directions, provenance areas and composition of lithic fragments in sandstones of the Qiangtang foreland basin during the Middle Jurassic to Early Cretaceous time, modified from Li *et al.* (2001).

Fig. 13. Cartoon of tectonic evolution of the Qiangtang Basin and adjacent terranes from Late Triassic to Cretaceous. The extent of each terrane is not strictly to scale and the near surface geometries are vertically exaggerated. The evolution models of Central Uplift during early Late Triassic (a) and Late Triassic-Early Jurassic (b) are modified after Zhang & Tang (2009). Bold black arrows in each cross sections represent the directions of sediment transportation. The mechanisms of subsidence are labelled in red.

Supporting material legends

File S1 Stratigraphic sections in the Qiangtang Basin in Google Earth format.

Table S1 Stratigraphic data of eleven composite sections in Qiangtang basin

Table S2 Age constraints from biostratigraphy of strata in Qiangtang basin

Table S3 GPS coordinates of AFT samples

Figure S1. Thermal history modeling results of samples from the Qiangtang Basin

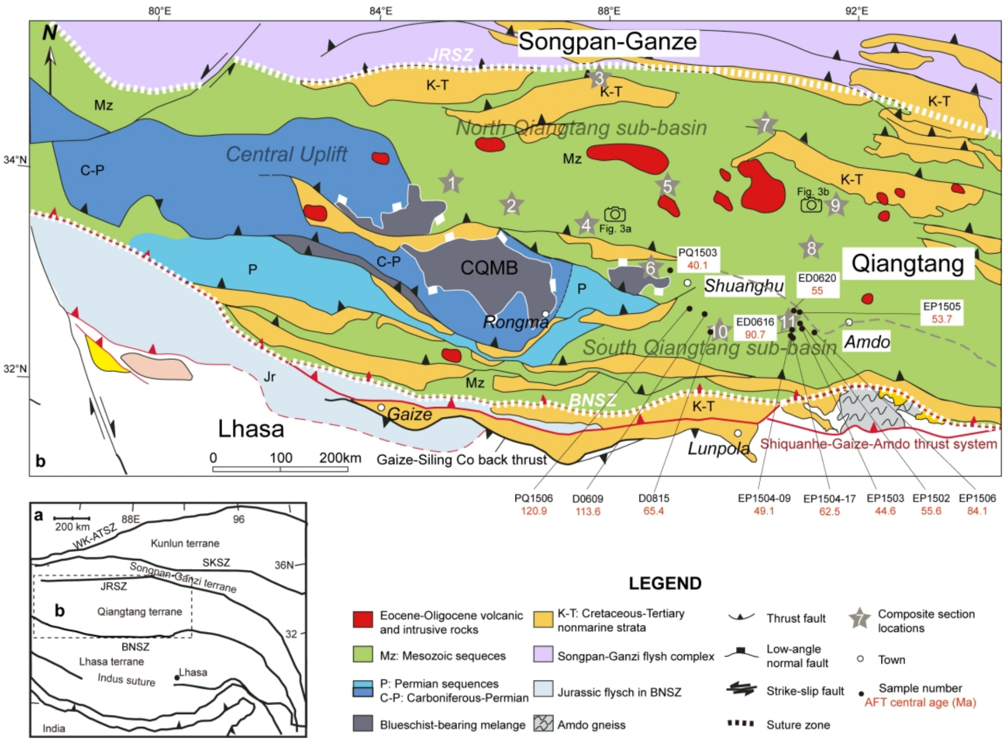

Fig. 1. a, Major terranes and sutures of the Tibetan plateau. b, Geological map of Qiangtang basin and adjacent terranes (modified after Kapp et al., 2005). WK-ATSZ = West Kunlun-Altyn Tagh suture zone; SKSZ = South Kunlun suture zone; CQMB = Central Qiangtang metamorphic belt; JRSZ = Jinsha River suture zone; BNSZ = Bangong-Nujiang suture zone. Numbers in grey stars represent the localities of composite sections: 1, Duxue Mt.; 2, Shuangquan Lake; 3, Heihuling; 4, Nadigangri; 5, Changshui River; 6, Amugang; 7, Zuerkenwula Mt.; 8, Dangmagang; 9, Quemo Co; 10, Biluo Co; 11, Dazhuoma.

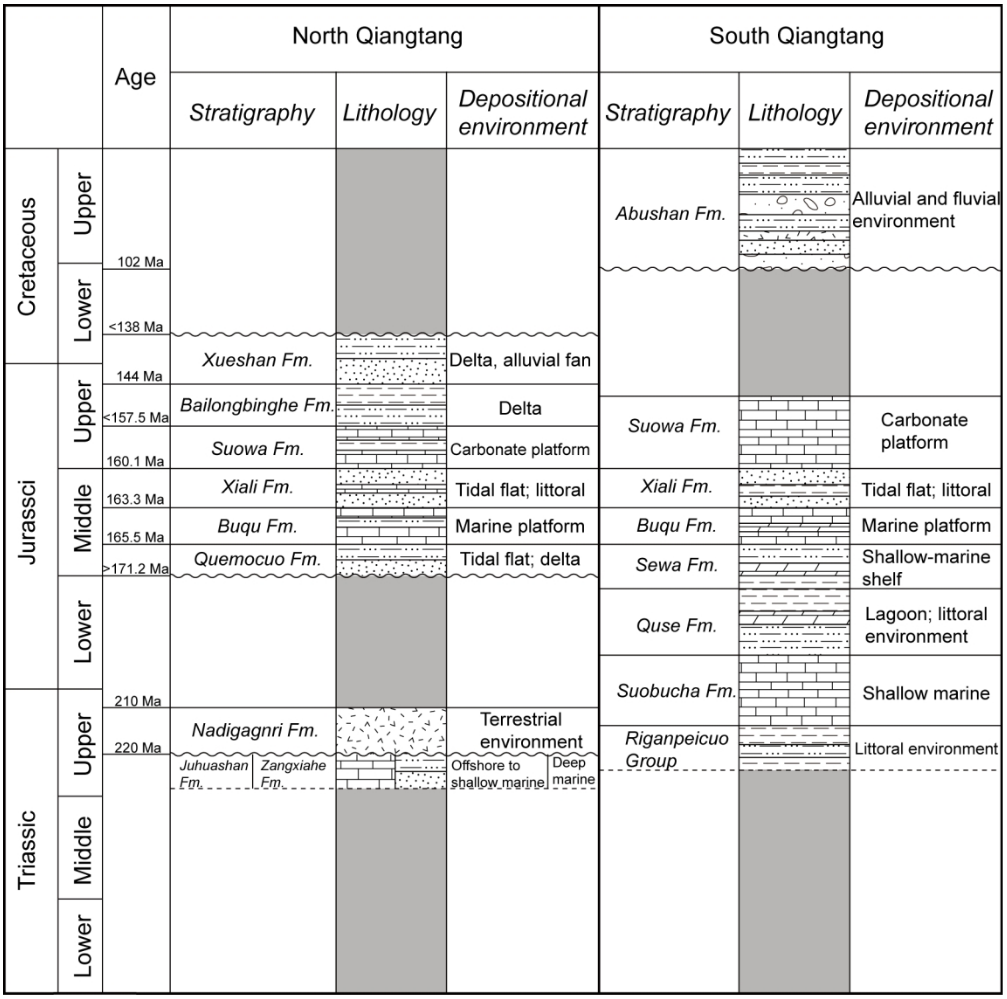

Fig. 2. Correlation of sequences, lithologies and paleo-environments of main Mesozoic stratigraphic units of the Qiangtang Basin. Not drawn to scale. The lithologies and interpretations of depositional environment of both the North and South Qiangtang are from field observations and geological reports. The age of Nadigangri Fm. comes from Zhai & Li (2007), Wang et al. (2008b) and Fu et al. (2010). Ages of Jurassic sequences are from magnetostratigraphy of Fang et al. (2016). The age of Abushan Fm. is from Li et al. (2015c). The legend of lithology is same to that of Fig. 4. All symbols are filled using patterns provided by U.S. Geological Survey (2006).

151x149mm (300 x 300 DPI)

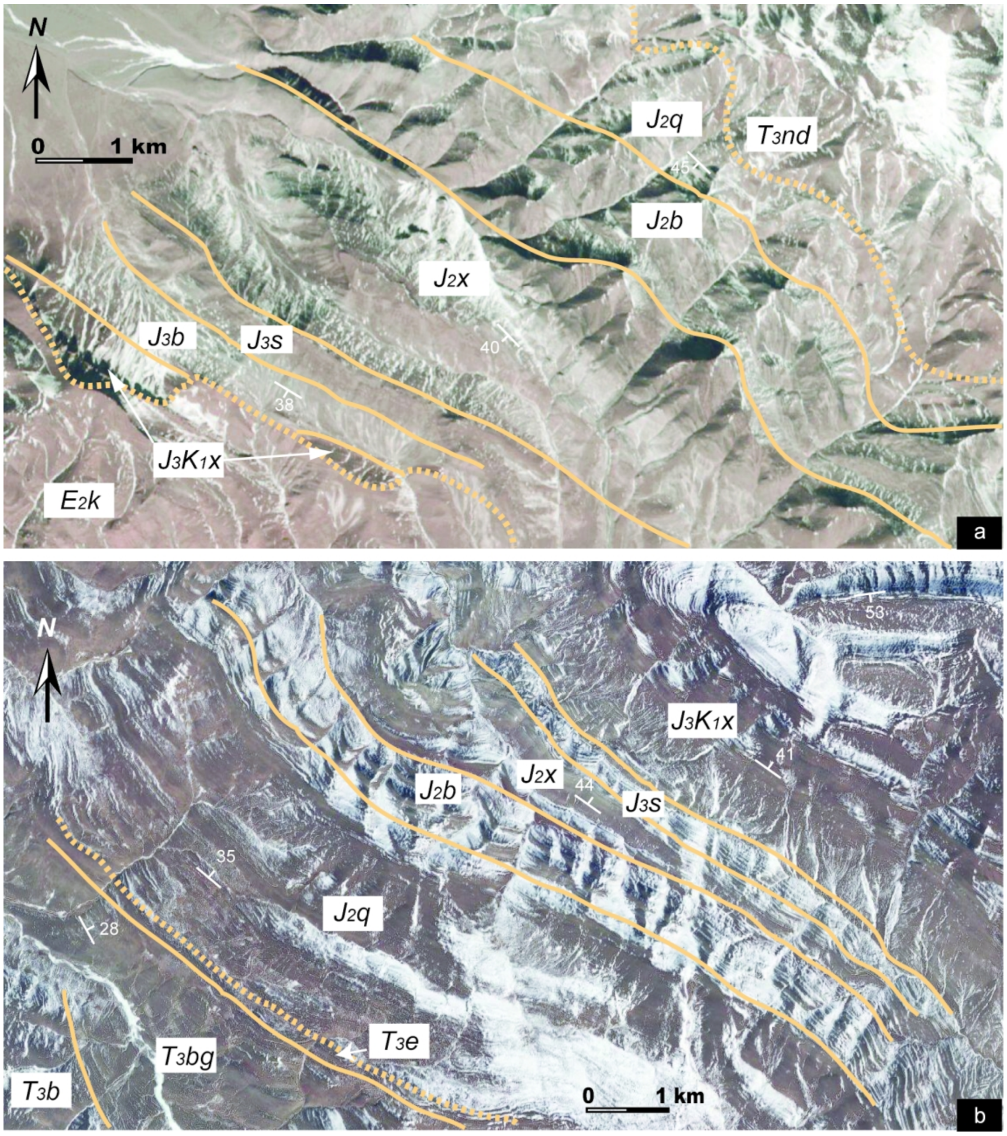

Fig. 3. Remote sensing images of specific profiles of continuous successions in Nadigangri (a) and Quemo Co (b) from Google Earth©. Structural dips are labelled on the strata. The solid lines are boundaries between stratigraphic units. The yellow dashed lines represent unconformities. T3nd = Nadigangri Formation; T3b = Bolila Formation; T3bg = Bagong Formation; T3e = Erlongba Formation; J2q = Quemocuo Formation; J2b = Buqu Formation; J2x = Xiali Formation; J3s = Suowa Formation; J3b = Bailongbinghe Formation; J3K1x = Xueshan Formation; E2k = Kangtuo Formation.

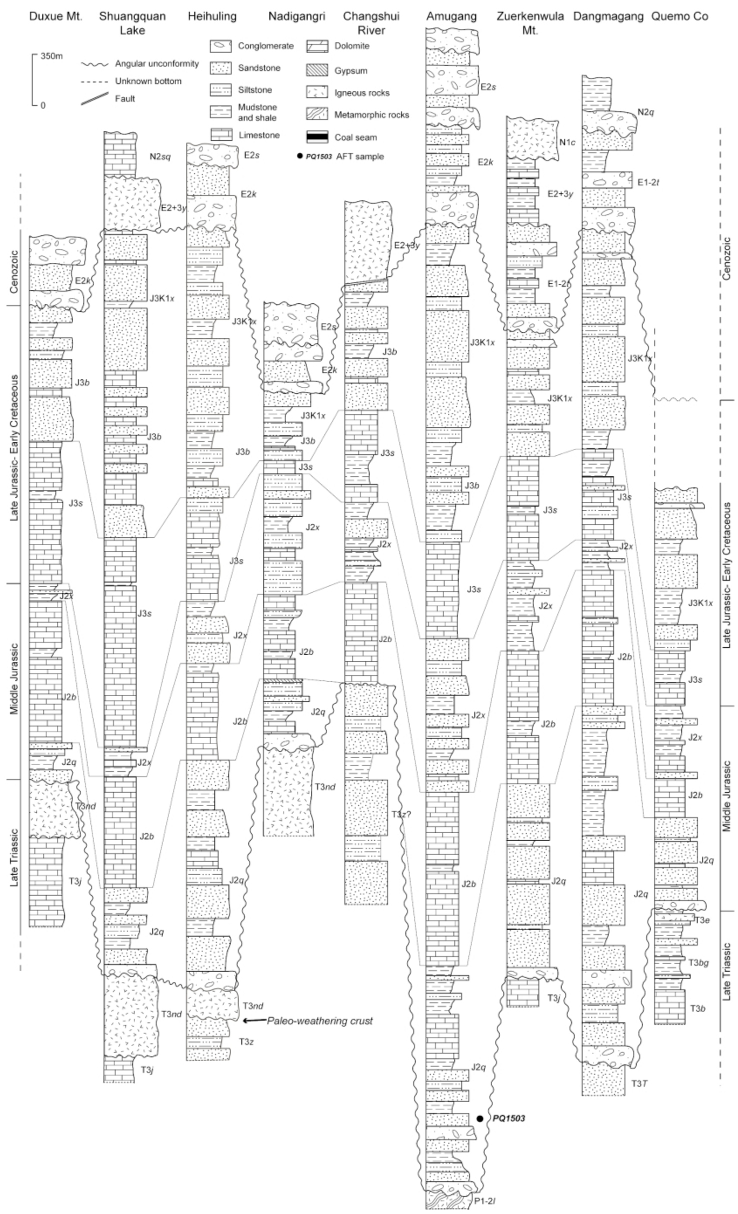

Fig. 4. Simplified stratigraphic framework of nine composite sections in the North Qiangtang sub-basin. The stratigraphic codes are same to those of Fig. 3. Other codes are: P1-2l = Lugu Formation; T3j = Juhuashan Formation; T3z = Zangxiahe Formation; T3T = Tumengela Group; E2s = Suonahu Formation; E1-2t = Tuotuohe Formation; E2+3y = Yulinshan Formation; N1c = Chabaoma Formation; N2q = Quguo Formation; N2sq = Shuangquanhu Formation.

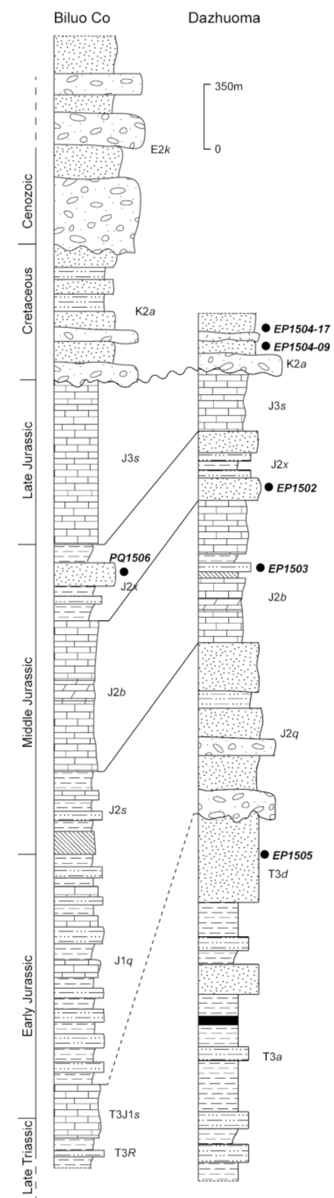

Fig. 5. Simplified stratigraphic framework of two composite sections in the South Qiangtang sub-basin. The legend, scale and stratigraphic codes are same to those of Fig. 4. Other codes are: T3a = Adula Formation; T3d = Duogaila Formation; T3R = Riganpeicuo Group; T3J1s = Suobucha Formation; J1q = Quse Formation; J2s = Sewa Formation; K2a = Abushan Formation.

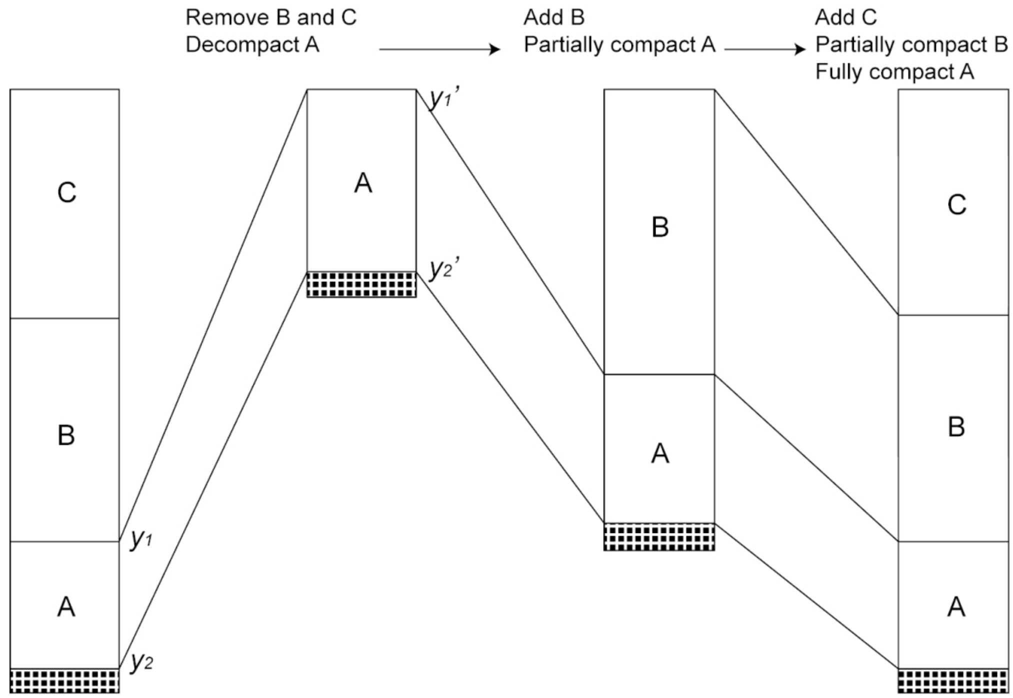

Fig. 6. Decompaction scheme (modified after Allen and Allen, 2005).

Fig. 7. Specific indicators for assessment of paleo-water depth in stratigraphic sections. (a) Oscillatory ripples preserved in the bottom of tidal sandstones (Late Triassic Duogaila Formation, Dazhuoma; paleo-water depth ≈ 50±50 m). (b) Fining-upward sequence with each starting with conglomerate or pebbled sandstones (Middle Jurassic Quemocuo Formation, Amugang; paleo-water depth ≈ 10±10 m). (c) Current bedding limestone (Middle Jurassic Quemocuo Formation, Amugang; paleo-water depth ≈50±50 m). (d) Ripples in tidal sandstones (Middle Jurassic Xiali Formation, Dazhuoma; paleo-water depth ≈50±50 m). (e) Ammonite in mudstone (Late Jurassic Bailongbinghe Formation, Changshui River; paleo-water depth ≈ 50 m). (f) Directional arrangement of gravels in fluvial sandstones (Late Cretaceous Abushan Formation, Biluo Co; paleo-water depth ≈ 10±5 m).

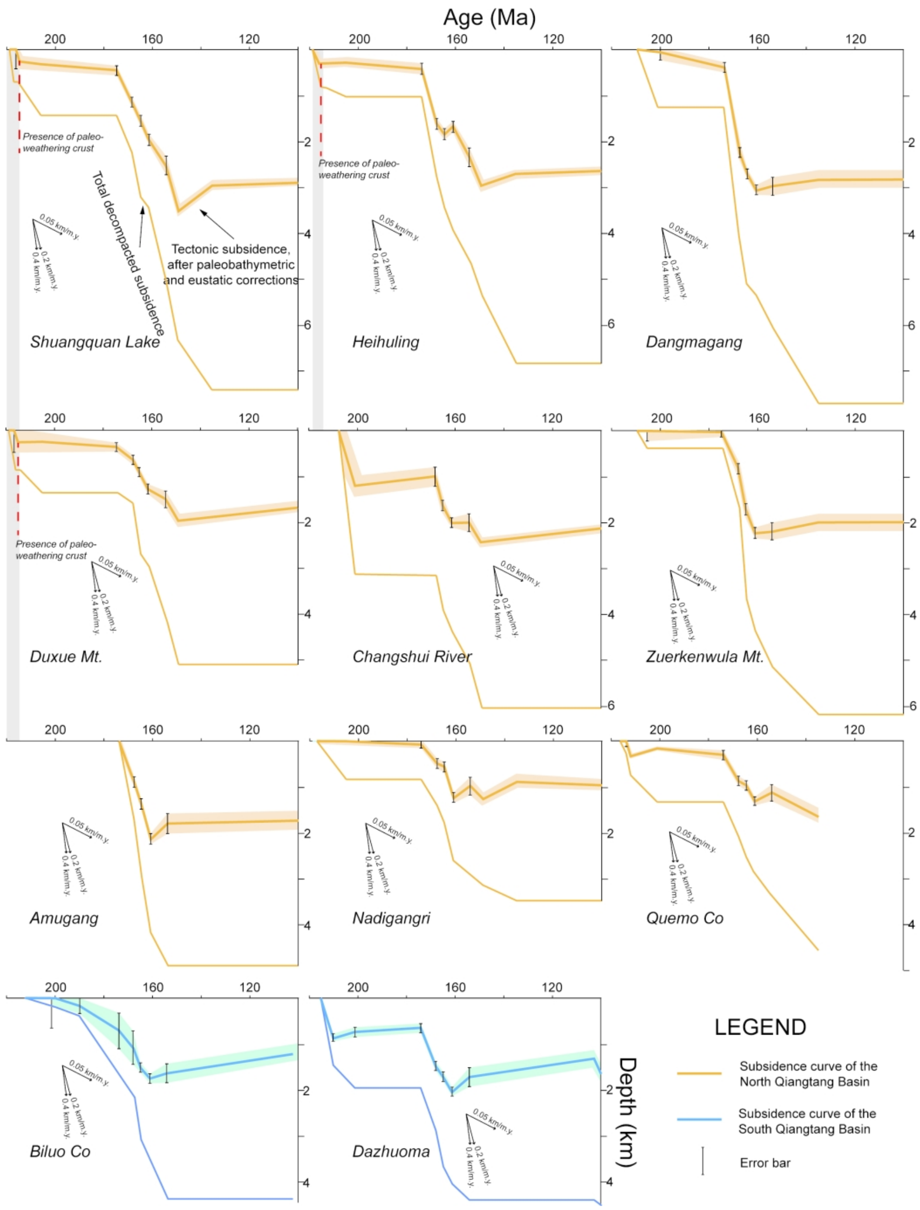

Fig. 8. Subsidence curves for composite sections in Fig. 1. The thick solid line represents backstripped tectonic subsidence. The thin solid line represents total decompacted subsidence. The grey-shade areas represent the first stage of subsidence from Late Triassic to Early Jurassic based on the subsidence histories, combined with previous work on sediment provenance and timing of deformation. The reference lines representing subsidence rate are shown are each of the plots.

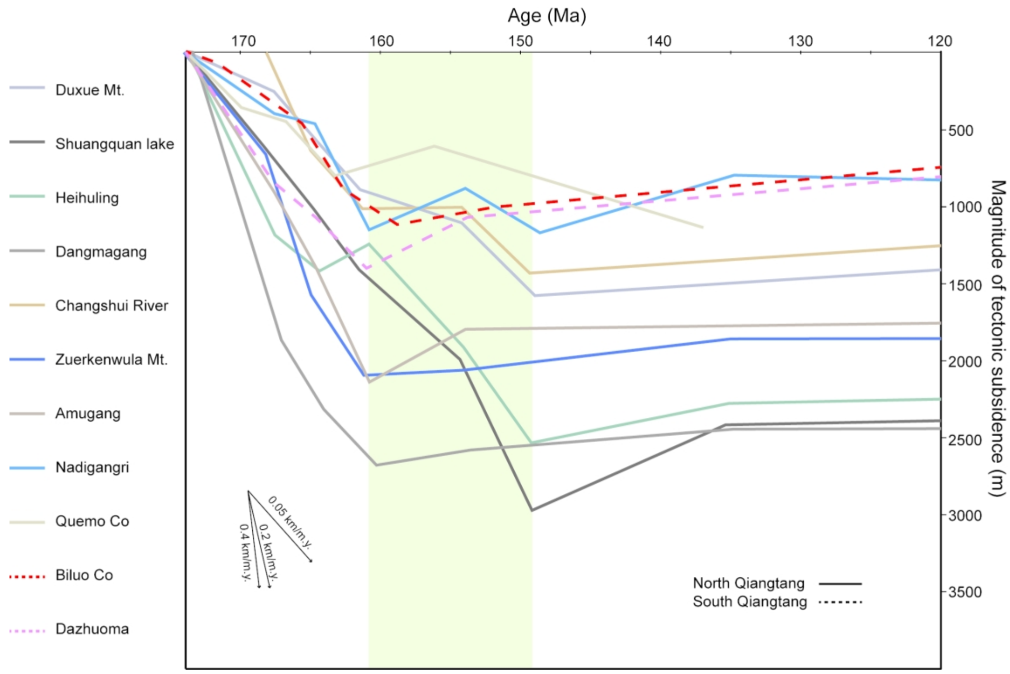

Fig. 9. Magnification of the tectonic subsidence histories from 172 to 120 Ma. The reference lines representing subsidence rate are shown are each of the plots. The shaded area represent the gradual cessation of subsidence across the Qiangtang Basin, with the final termination at about 148 Ma. The subsidence curves in the North Qiangtang are represented by solid lines, while the South Qiangtang are represented by dotted lines.

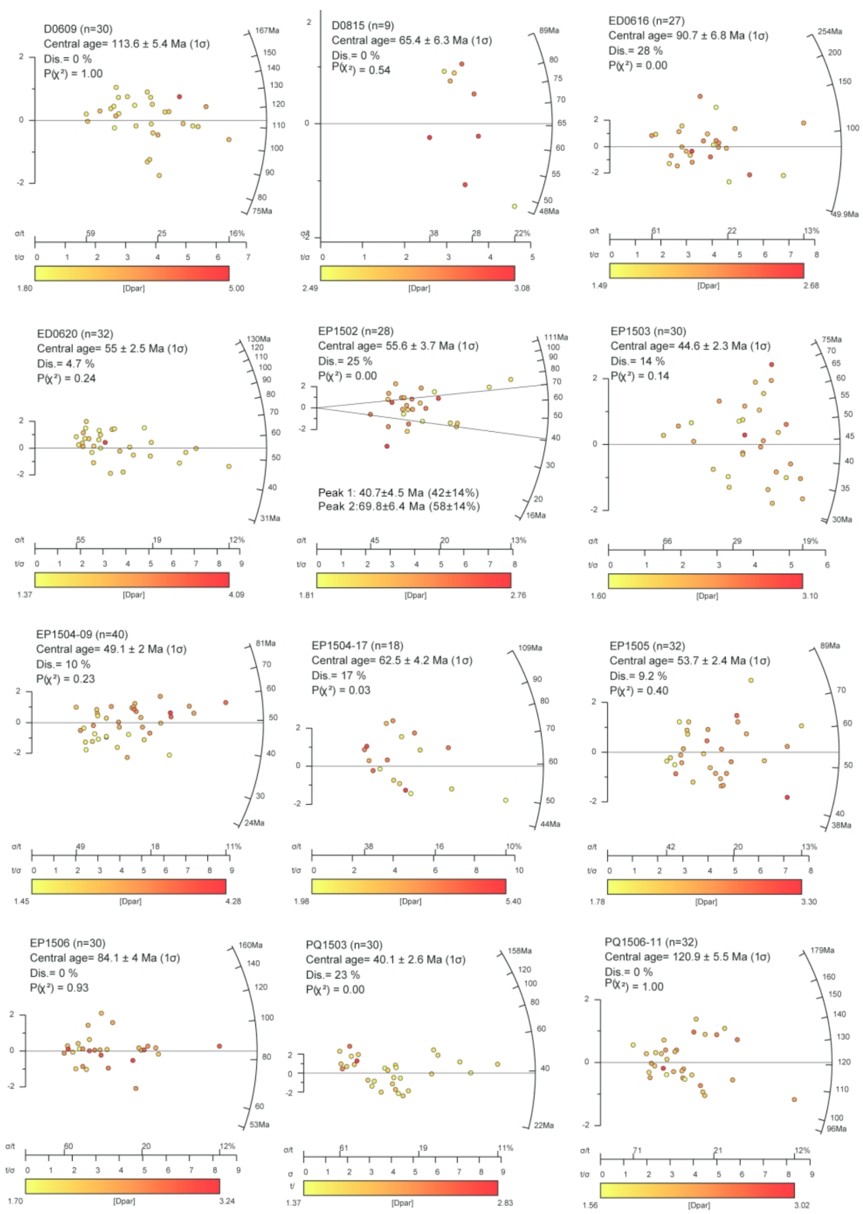

Fig. 10. Radial plots of detrital apatite fission track ages in the Qiangtang Basin using DensityPlotter (Vermeesch, 2012).

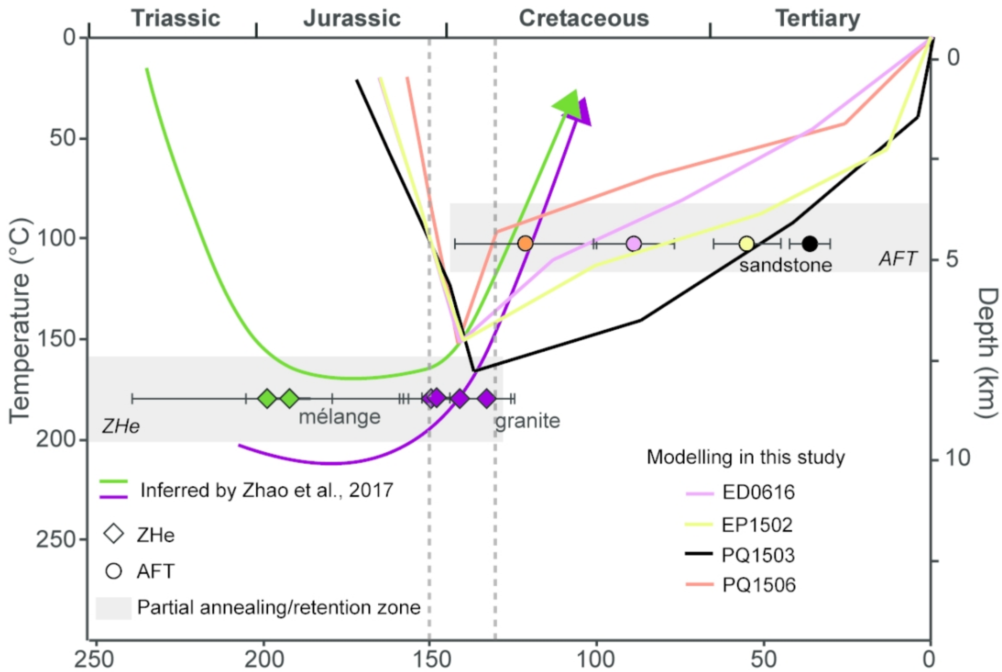

Fig. 11. Weighted mean thermal paths for sandstones in the Qiangtang Basin. The mélange and granite samples are from the Central Uplift studied by Zhao et al. (2017). All thermal paths display cooling starting from 150-130 Ma. The depth is calculated by assuming a geothermal gradient of 20 °C/km.

104x70mm (300 x 300 DPI)

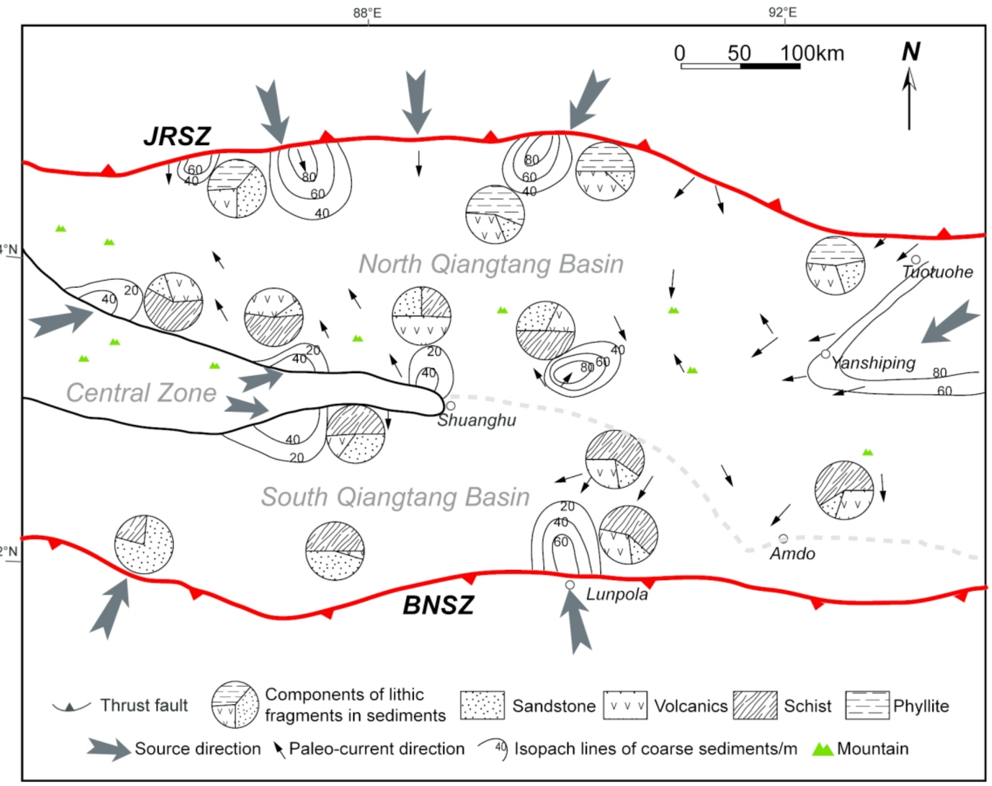

Fig. 12. Schematic map showing the paleo-current directions, provenance areas and composition of lithic fragments in sandstones of the Qiangtang foreland basin during the Middle Jurassic to Early Cretaceous time, modified from Li et al. (2001).

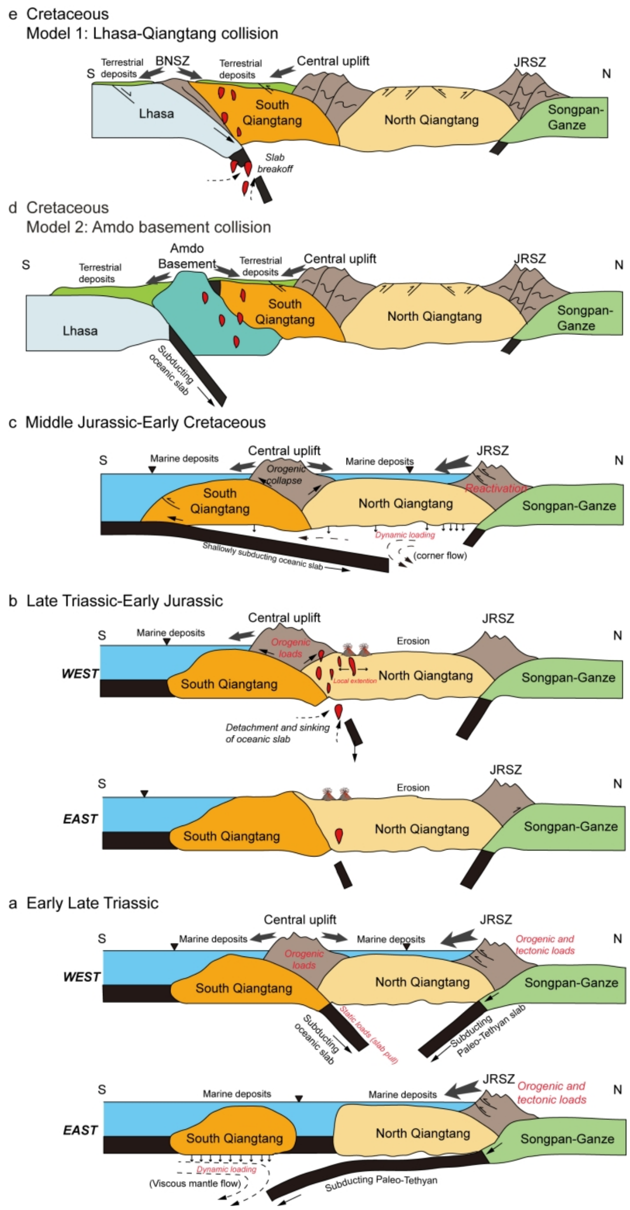

Fig. 13. Cartoon of tectonic evolution of the Qiangtang Basin and adjacent terranes from Late Triassic to Cretaceous. The extent of each terrane is not strictly to scale and the near surface geometries are vertically exaggerated. The evolution models of Central Uplift during early Late Triassic (a) and Late Triassic-Early Jurassic (b) are modified after Zhang & Tang (2009). Bold black arrows in each cross sections represent the directions of sediment transportation. The mechanisms of subsidence are labelled in red.